Frequency Domain Fluorescent Molecular Tomography and Molecular Probes for Small Animal Imaging

---

A Dissertation

Presented to

The Faculty of the Graduate School

University of Missouri, Columbia

In Partial Fulfillment

Of the Requirements for the Degree

Doctor of Philosophy

By

NARESH GANDHI KUJALA

Dr. Ping Yu
Dissertation Supervisor

JULY 2009

The undersigned, appointed by the Dean of the Graduate School, have examined the dissertation write up entitled:

Frequency Domain Fluorescent Molecular Tomography and Molecular Probes for Small Animal Imaging

Presented by NARESH GANDHI KUJALA

A candidate for the degree of Doctor of Philosophy, and hereby certify that, in their opinion, it is worthy of acceptance.

_____
Dr. Ping Yu

_____
Dr. H. R. Chandrasekhar

_____
Dr. Meera Chandrasekhar

_____
Dr. Lixin Ma

_____
Dr. Shi-Jie Chen

Dedicated to my parents:

Kujala Narasimha and Bhanumathi

Dedicated to my wife, son and daughter:

Kujala Siriyala, Saichandra, and Medha

ACKNOWLEDGEMENTS

I would like to thank my supervisor Dr. Ping Yu, Assistant Professor of Physics and Astronomy, for his support, encouragement and guidance throughout the whole period of my Ph.D. studies. He provided superior guidance, and I have the deepest respect for him. I am forever indebted to him. I learned something new every time I talked with him. It has been a great privilege to know him and his examples have been highly motivating.

I am grateful to Dr. Lixin Ma, Assistant Professor in the Department of Radiology, for her help in the development and evaluation of the MRI-Optical imaging of molecular probes. I appreciate her support and suggestions to me. She had a great deal of patience in answering my questions and clarifying my understanding. She engaged me in discussions that resulted in new ideas. I am honored to have her as my external committee member and co-advisor.

I must express my gratitude to my committee members Dr. Meera Chandrasekhar, Dr. H. R. Chandrasekhar, and Dr. Shi-Jie Chen for their support and valuable suggestions in my doctoral work.

I would like to express my thanks to Dr. Mark Milanick, Professor, Department of Medical Pharmacology and Physiology, at the Dalton Cardiovascular Research Center for his financial support of my doctoral program, through the Clinical BioDetective Program funded by NIH.

I am thankful to Dr. Esteban Fernandez, Associate Director of the Molecular Cytology Core at the Life Sciences Center at the University of Missouri for assistance in my *in vitro* studies of the molecular probe, using confocal and fluorescent microscopy. I am thankful to Dr. J C Hebden, Department of Medical Physics and Bioengineering, University College of London, London for lending us conical tissue phantoms for calibration and testing our system.

I am grateful to Marianne, Lora, Sarah, and Gay in the Department of Physics and Astronomy for their valuable assistance in my visa paperwork. I am thankful to Sam Potts for helping in the design and machine work for the filter set design for our project. I would like to express my thanks to Dr. Jeff Smith, Dr. Tim Hoffman, Gary and the staff of the Biomolecular Imaging Center at the VA Hospital for the synthesis of the Alexa fluor 680 and Alexa fluor 750 bombesin molecular probes.

I would like to thank Dr. Chen Yu, Assistant Professor of Physics at the University of Maryland, and Dr. Sudarshan Loyalka, Professor of Nuclear Engineering at the University of Missouri, for their support and valuable discussion of the project.

I thank my group members Haibo, Linghui, Yve, Dr. Sunder, Dr. Zhang, Brian, Domingo, Adam, Huifang, and Ashley for their enduring support and regular fruitful discussions and the invaluable transfer of knowledge. I am grateful to my friends Raghuveer, Sandy, Shawn Hayden, Jagat, Ranjith, Venkat, Amar and my brother Ram Narayan Rao for their help and support. I am thankful to Melissa Poole for her editorial assistance in proofreading my dissertation.

Finally, I would like to express my heartfelt gratitude to my parents for their support of my pursuit of a Ph.D. I would like to dedicate this work to my wife, son, and daughter.

TABLE OF CONTENTS

LIST OF FIGURES

Figure **Page**

Chapter 2:

Chapter 3:

LIST OF ABBREVIATIONS

AF	Alexa Fluor
AC	Alternating Current
BBN	Bombesin
BF	Bandpass Filter
CCD	Charge Coupled Device
CW	Continuous Wave
CT	Computed Tomography
DPDW	Diffuse Photon Density Wave
DAQ	Data Acquisition Card
DOT	Diffuse Optical Tomography
DC	Direct Current
Ex	Excitation
Em	Emission
FOV	Field of View
FMT	Fluorescent Molecular Tomography
FDPM	Frequency Domain Photon Migration
FD	Frequency Domain
GRP	Gastrin Releasing Peptide
GRPr	Gastrin Releasing Peptide receptor
IF	Intermediate Frequency
LF	Longpass Filter

LO	Local Oscillator
LD	Laser Diode
MRI	Magnetic Resonance Imaging
MRS	Magnetic Resonance Spectroscopy
MW	Molecular Weight
NIR	Near-infrared
ns	Nanosecond
ND	Neutral Density
NA	Numerical Aperture
PET	Positron Emission Tomography
Ps	Picoseconds
PMT	Photomultiplier Tube
RF	Radio Frequency
Rx	Receiver
RMS Voltage	Root Mean Square Voltage
SCID	Severely Comprised Immunodeficient
SPECT	Single Photon Emission Computed Tomography
SNR	Signal-to-Noise
TD	Time Domain
Tx	Transmitter
TDPM	Time Domain Photon Migration
TPSF	Temporal Point Spread Function
US	Ultrasound

ABSTRACT

Fluorescent molecular tomography (FMT) is a noninvasive biomedical optical imaging that enables 3-dimensional quantitative determination of fluorochromes distributed in biological tissues. There are three methods for imaging large volume tissues based on different light sources: (a) using a light source of constant intensity, through a continuous or constant wave, (b) using a light source that is intensity modulated with a radio frequency (RF), and (c) using ultrafast pulses in the femtosecond range. In this study, we have developed a frequency domain fluorescent molecular tomographic system based on the heterodyne technique, using a single source and detector pair that can be used for small animal imaging.

In our system, the intensity of the laser source is modulated with a RF frequency to produce a diffuse photon density wave in the tissue. The phase of the diffuse photon density wave is measured by comparing the reference signal with the signal from the tissue using a phasemeter. The data acquisition was performed by using a Labview program.

The results suggest that we can measure the phase change from the heterogeneous inside tissue. Combined with fiber optics and filter sets, the system can be used to sensitively image the targeted fluorescent molecular probes, allowing the detection of cancer at an early stage.

We used the system to detect the tumor-targeting molecular probe Alexa Fluor 680 and Alexa Fluor 750 bombesin peptide conjugates in phantoms as well

as mouse tissues. We also developed and evaluated fluorescent Bombesin (BBN) probes to target gastrin-releasing peptide (GRP) receptors for optical molecular imaging. GRP receptors are over-expressed in several types of human cancer cells, including breast, prostate, small cell lung, and pancreatic cancers. BBN is a 14 amino acid peptide that is an analogue to human gastrin-releasing peptide that binds specifically to GRPr receptors. BBN conjugates are significant in cancer detection and therapy. The optical molecular probe AF750 BBN peptide exhibits optimal pharmacokinetic properties for targeting GRPr in mice. Fluorescent microscopic imaging of the molecular probe in PC-3 prostate and T-47D breast cancer cell lines indicated specific uptake, internalization, and receptor blocking of these probes. *In vivo* investigations in severely compromised immunodeficient (SCID) mice bearing xenografted PC-3 prostate and T47-D breast cancer lesions demonstrated the ability of this new molecular probe to specifically target tumor tissue with high selectively and affinity.

Chapter 1

Overview

1.1 Introduction

We have developed a frequency domain fluorescent molecular tomographic system based on a heterodyne technique with a near infrared wavelength for 3-dimensional molecular imaging in small animals. In a frequency domain fluorescent molecular tomographic system, the phase of the fluorescence density wave is used to determine the location of the molecular probe. Our system, based on the frequency domain heterodyne method and 3-dimensional reconstruction, can provide phase measurement with very high accuracy. It can be used to detect the molecular targeting process of fluorescent probes.

This system has great potential for diagnostic molecular imaging. The use of near-infrared light can provide functional information within tissues. It has enormous potential for molecular imaging, particularly when coupled with near-infrared excitable molecular probes. Conventional biomedical imaging systems can detect anatomical changes and physiological changes resulting from diseases. With optical molecular imaging, however, we can detect the active molecular pathways of disease in the tissue before anatomical and physiological changes appear. This form of imaging can be used to detect disease at very early stages.

We have also developed and evaluated molecular probes, based on Bombesin (BBN) peptide, that specifically target the gastrin releasing peptide receptor (GRPr) over-expressing in several cancer cell lines. The molecular probes are synthesized using Bombesin and two fluorescent molecules: Alexa Fluor 680 and Alexa Fluor 750. *In vitro* cellular experiments and *in vivo* small animal experiments confirm the normal uptake and internalization of newly-developed probes for prostate and breast cancer cells. Phantom tissues were developed, based on the fluorescent probes, and used to evaluate our molecular imaging system.

The probe development work was performed at the Biomolecular Imaging Center, Harry S. Truman Veterans (VA) Hospital under the supervision of Dr. Lixin Ma. The optical fluorescence imaging studies of small animals, using molecular probes with Alexa Fluor 680 and Alexa Fluor 750, were also performed at the Biomolecular Imaging Center on Xenogen IVIS 200 fluorescence/bioluminescence imaging system. The phantom tissues were prepared at the chemistry lab in the VA Hospital.

The optical imaging system at the Department of Physics and Astronomy at the University of Missouri was designed specifically for multimodal imaging that combines the multi-wavelength near-infrared fluorescent tomography with micro-magnetic resonance imaging (MRI) to study breast cancer and prostate cancer in small animal models. The fiber detection of the optical imaging system is compatible with highly magnetic fields inside MRI scanners. With multimodal

FMT/MRI images and high-resolution images from the MRI, we can achieve highly sensitive optical imaging to determine optical and chromophore properties.

1.2 Motivation and Research Objectives

Molecular imaging is a rapidly developing field in biomedical research. In small animal imaging, it has potential for non-invasively interrogating animals in disease progression, evaluating the effects of drugs, assessing the pharmacokinetic behavior of a drug, and identifying molecular biomarkers [1-5]. A prerequisite of molecular imaging is the development of specific, targeted imaging contrast agents to assess biological processes. The selection of contrast agents depends on the physical principles of the imaging modality. Optical imaging has very high sensitivity and relatively low cost. Several optical methods have been applied to small animal molecular imaging studies, including bioluminescence, fluorescent proteins, and fluorochrome-labeled agents. Fluorochrome-labeled agents have potential for human clinical applications [6, 7].

Fluorescent molecular tomography is an emerging *in vivo* imaging technique that resolves the problems of bio-distribution of fluorescent probes for specific cellular and sub-cellular targets. It can be used for cancer diagnosis, where early detection is critical. With near-infrared excitable fluorescent molecules, probes can be synthesized with the conjugation of specific peptides targeting cancer cells. The fluorescent molecular tomography system can detect a near-infrared fluorescent probe embedded in deep tissues in a small amount

(pico-mole scale), which allows early detection and molecular target assessment of cancerous tissue. This system also allows three-dimensional localization in deep tissues and quantification of molecular probes with specific targeted cancer cells.

The primary goal of optical molecular imaging is to develop a diagnostic imaging modality based on the near-infrared (700-1000nm) wavelength. This process offers several advantages over existing imaging modalities. The wavelength selection is very important for tissue imaging. For optical imaging in the visible wavelength range, absorption in tissue is dominated by deoxy-hemoglobin and oxy-hemoglobin. When the wavelength is extended into the middle-infrared range, water absorption dominates the tissue optical properties.

The near-infrared wavelength provides a window for optical imaging in which the main mechanism of photon-tissue interaction is scattering. Near-infrared photons can penetrate deeper into tissue; this technique can provide functional information about the tissue, such as blood content, oxygenation, and the presence of water and lipids.

Molecular probes, biomarkers, and optical contrast agents were developed that can be specifically and selectively bound to the target vector with high binding affinity; they also can be imaged using the fluorescent molecular tomographic system. The near-infrared fluorescent probes can also be used to overcome the problem of auto fluorescence from organs such as the stomach, kidneys, and bladder, which makes it difficult to distinguish normal tissue from cancerous tissue [8, 9, 10].

We have developed molecular probes to specifically bind prostate and breast cancerous cells. Cancer receptors that can bind target vectors with molecular imaging probes and radiopharmaceuticals offer a means for early detection and targeted therapeutic interventions through recognition of receptors uniquely over-expressed in human cancer cells.

Bombesin is 14-amino acid peptide that shows high binding affinity and specificity for gastrin releasing peptide receptors (GRPr). The GRPr is over-expressed in many human cancer cell lines, including breast, prostate, colon, and small cell lung cancers. In this study we applied optical imaging methods to investigate the conjugate uptake and blocking in cancer cells and tumor bearing mice. We have made significant progress in molecular imaging in the development of fluorophores in the near-infrared range (700nm-900nm), with high quantum efficiency, chemical and optical stability, and suitable pharmacological properties [11, 12, 13].

Bibliography:

1. Gambir SS, Barrio JR, Phelps ME, et al. “Imaging adenoviral-directed reporter gene expression in living animals with positron emission tomography”. Proc Natl Acad Sci USA, Vol. 96, 2333-2338 (1999)

2. Weisslder R, Tung CH, Mahmood U, Bogdanov A Jr. “In vivo imaging of tumors with protease-activated near-infrared fluorescent probes”. Nat Biotechnol, Vol. 17, 375-378 (1999)

3. Kwon S, Ke S, Houston JP, Wang W, Wu Q, Li C, Sevick-Muraca EM. “Imaging dose-dependent pharmacokinetics of an RGD-fluorescent dye conjugate target to alpha v beta 3 receptor expressed in Kaposi’s sarcoma”. J Mol Imaging, Vol. 4, 75-87 (2005)

4. Cheng Z, Wu Y, Xiong Z, Gambir SS, Chen X. ”Near-infrared fluorescent RGD peptides for optical imaging of integrin alphavbeta3 expression in living mice”. Bioconjugate Chem, Vol. 16, 1433-1441 (2005)

5. Petrovksy A, Schellenberger E, Josephson L, Weissleder R, Bogdanov A Jr. “Near-infrared fluorescent imaging of tumor apoptosis”. Cancer Res, Vol. 63, 1936-1942 (2003)

6. Amersham GE (www.gelifesciences.com) and Li-Cor Biosciences (www.licor.com).

7. Khazaie K, Schirrmacher V, Lichtner RB. ”EFG receptor in neoplasia and metastasis”, Cancer Metastasis Rev, Vol. 12, 255-274 (1993)

8. Weissleder R. “Molecular imaging in cancer”. Science, vol. 312, 1168-1171 (2006)

9. Hawrysz DJ, Sevick-Muraca EM. “Developments towards diagnostic breast cancer imaging using near-infrared optical measurements and fluorescent contrast agents”. Neoplasia, Vol. 2, 388-417 (2000)

10. Frangioni JV. “In vivo near-infrared fluorescence imaging”. Curr Opinion Chem Bio, Vol. 7, 626-634 (2003)

11. Licha K, “Contrast agents for optical imaging”. Curr. Topics Chem, Vol. 222, 1-29 (2002)

12. Gurfinkel M. Ke S, Wen X, Li C, Sevick-Muraca EM. “Near-infrared fluorescence optical imaging and tomography”. Disease Markers, Vol. 19, 107-121 (2004)

13. Ma L, Yu P, Veerandra B, Rold TL, Retzloff L, Prasanphanich A, Sieckman G, Hoffman T, Volkert W, Smith J. ”In vitro and In vivo evaluation of alexa fluor 680-BBN [7-14]NH2 peptide conjugate: A high affinity fluorescent probe having high selectivity for the GRP receptor”. Molecular Imaging, Vol. 6(3), 171-180 (2007)

Chapter 2

Fluorescence Density Waves and Frequency Domain Heterodyne System

2.1 Introduction and Background

Near infrared biomedical optical imaging technologies offer several distinct advantages in sensitivity to functional changes and non-ionized radiation; they are also less costly and more user friendly than other biomedical imaging techniques [1, 2]. The transportation of light in tissue can be described and measured through Maxwell's equations, Monte Carlo simulations, Mie scattering theory, and radiation transportation theory [3, 4]. In recent years, photon migration theory has attracted more and more attention in diffusion approximation [5, 6, 7]. Experimental techniques associated with this theory have been developed. The important feature of near infrared measurement is that it can be used to image a large volume of tissues. It also has the ability to provide functional information, such as tissue oxygenation, water and lipid content by absorption coefficient, and the scattering coefficient, using the Beer-Lambert law and diffusion theory. These features, however, are based on optical properties of biological tissue.

One technique that has become popular in recent years is using exogenous fluorescent dyes to improve signal-to-noise contrast and targeting

specific vectors to detect small inclusions of disease in thick and deep tissues [8, 9, 10 and 11]. The benefit of using exogenous fluorescent dyes is that it is possible to provide very sensitive detection of physiological changes inside biological tissue. This new direction encourages the development of a fluorescent molecular tomographic system that allows robust imaging of specific molecular targets in vivo. This technique has the potential for widespread applications in biology and clinical medicine. Molecular imaging based on fluorescent molecular tomography can be used to detect near-infrared fluorophore embedded inside tissue that yields high fluorescence contrast and allows early detection and molecular targeting and assessment of cancerous tissues. Given current research and progress in molecular imaging technology, we expect that molecular imaging diagnosis will be applied in patient care within the next 5 years.

2.2 Interaction of Biological Tissue with Near-infrared Light Photons

The interaction of biological tissue with near-infrared light photons depends on characteristics of the tissue. Due to the highly inhomogeneous properties of cells inside tissue, the photons experience random movement that is mathematically treated as transportation or diffusion. Although the migration of a single photon inside tissue cannot be traced, the optical properties of a tissue are primarily described by absorption and scattering of a large number of photons.

2.2.1 Absorption

The attenuation of light through a non-scattering medium can be attributed to the absorption of photons by the medium. If a medium is non-scattering and illuminated by light of intensity I_0, the intensity of the emerging light will be determined by the Beer-Lambert law:

$$I = I_0 e^{-\mu_a l}$$

where μ_a is the absorption coefficient of the medium and l is the thickness of the sample. The absorption coefficient shows the probability of the photons being absorbed by the medium per unit length. and the number of absorbing substances, like chromophores and lipids. The individual extinction coefficients of each chromophore represent their absorption at a particular concentration. The absorption coefficient of chromophores is expressed as the sum of products of concentration of each chromophore with its extinction coefficient.

2.2.2 Scattering

The scattering properties of a medium are described by its scattering coefficient $\mu_{s,}$ the product of the density of scattering particles and the scattering cross section. The scattering coefficient represents the probability per unit length of a photon being scattered. Attenuation through a simple scattering medium can be described by the modified Beer Lambert law. Light propagation through more complex scattering tissue can be described both analytically and numerically by using the Radiative Transfer Equation (RTE). In special cases, scattering media have optical anisotropy. The scattering properties of bulk media are often

described in terms of the reduced scattering coefficient μ'_s. The light photons generally emerge in a preferential direction relative to their incident angle. The anisotropy of the scatter is given by the mean cosine or Landé g-factor to describe simple directional effects. The reduced scattering coefficient, $\mu'_{s,}$ is given by following equation:

$$\mu'_s = \mu_s(1-g)$$

The scattering cosine function depends on the size, shape, and refractive index of scattering particles. If g=0, the scattering is isotropic; when g=1, the scattering is entirely forward.

Figure 2.1 demonstrates the wavelength-dependent absorption coefficient of biological tissues and hemoglobin in the wavelength range of 100nm to 1000nm. Hemoglobin, water, melanin, and lipids have relatively low absorption in the infrared wavelength. However, the wavelength in the visible range for hemoglobin, melanin, and lipids has a high absorption coefficient. Water also has increased absorption in the visible wavelength range. Absorption of biological tissues in the near infrared can be neglected. From this property of tissue, the RTE equation can be simplified to the diffusion equation, making a simple analytical solution solve the absorption coefficients and scattering coefficients of tissues. Therefore, the near infrared wavelength could be a “window” for the light photons migrating to a longer distance before being absorbed by tissue.

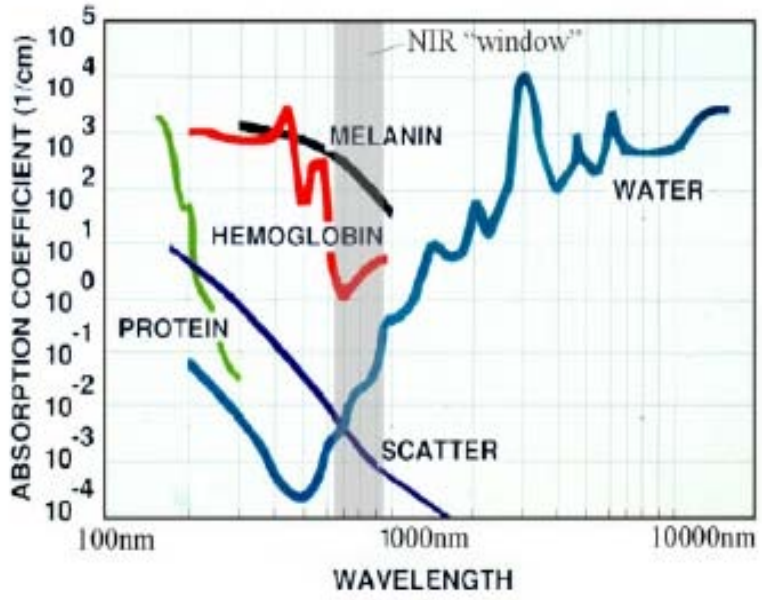

Figure 2.1: The absorption coefficient of hemoglobin, water and lipids as a function of wavelength (Courtesy of Elizabeth Hillman, et al, ref. 25).

2.3 Different Methods of Optical Imaging

Commonly, there are three near-infrared optical imaging methods for biomedical optical tomography: the continuous wave (CW) method, the time-domain photon migration (TDPM) method, and the frequency-domain photon migration (FDPM) method [25, 29, and 32]. These methods have been developed for imaging deep tissue volumes from surface measurements.

2.3.1 Continuous Wave Method

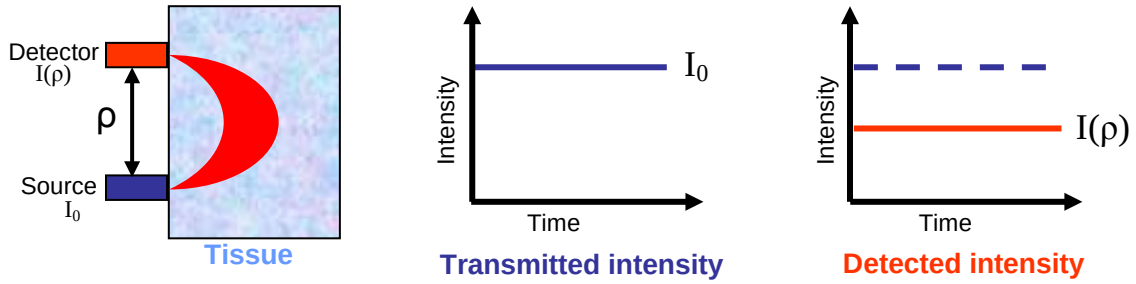

Figure 2.2: Schematic of a continuous wave method. The continuous wave is incident on tissue medium; and the detected intensity is attenuated with the position of the detector.

The continuous wave system for NIR optical tomography is the wavelength dependent attenuation of the emerging light that can be measured. In a continuous wave system, the light source has constant amplitude and frequency and has a constant intensity incident on tissue. The detected intensity will decrease dependent on the source-detector locations, as shown in figure 2.2. The amplitude and frequency are constant when continuous wave propagate in tissue. By using the Beer-Lambert law, the absorption and scattering changes can be calculated from the attenuation changes. Arridge et al, Meet et al, and Springett et al, [12] have shown this technique is often used to acquire volume and single-point measurements of tissue samples and time-series changes in functional parameters in the cerebral cortex.

The continuous wave (CW) imaging technique in biomedical medical applications can be used to study haemodynamic and oxygenation changes in

tissues and in the outer (cortical) regions of the brain. For instance, Schmitz et al and Barbour et al [27] have demonstrated a CW tomography system that uses gating and averaging the detected signals to reveal cyclic haemodynamic changes. However, there are some disadvantages associated with CW imaging using absolute measurement of intensity. Intensity measurements are far more sensitive to the optical properties of tissues at or immediately below the surface than localized regions deeper within the tissue. The detected intensity is also highly dependent on surface coupling. Finally, measurements of intensity alone at a single wavelength are unable to distinguish between the effects of absorption and scatter and between changes in blood volume and oxygenation [14]. (4) The tissues that highly scatter media photons can take one or many different paths from the source to the detector located at the air-tissue interface.

The continuous wave techniques have no means of detecting the distribution of the photon path lengths; they are limited in the amount of information they can provide for imaging interior optical properties. However, the continuous wave systems are simpler than that of time-domain and frequency-domain systems, as they consist of only CW light sources and intensity detectors.

2.3.2 Time Domain Method

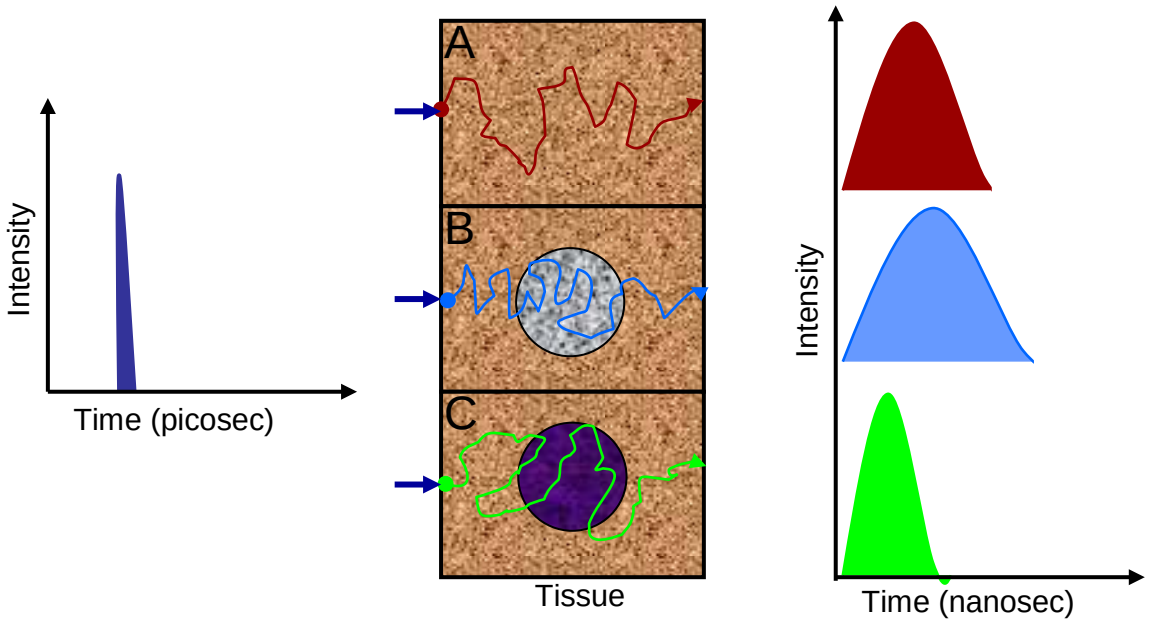

Figure 2.3: Schematic of a time domain method. The pulse laser (picoseconds) provides incident intensity and pulse signal (nanoseconds) is detected from the tissue. (A) Represents the tissue medium without any absorption and scattering heterogeneous, (B) Represents the tissue medium with scattering heterogeneous (C) Represents the tissue medium with absorption of heterogeneous.

The time domain method measures the time taken for individual photons to propagate through tissues. This can be achieved with a pulsed light propagating through the tissue, using fast detectors to record how the pulse has been broadened when it emerges. The time domain method utilizes a short pulse and the broadening of the light pulse, due to the multiple scattering, as shown in figure 2.3. The broadened pulse (referred as a temporal point spread function

(TPSF)) is represented by a histogram of the time each photon took to travel from the source to the detector with scattering and absorbing mechanisms in the tissue. After traveling through several centimeters of soft tissue, the TPSF will extend over several nanoseconds [15]. To determine the distribution of photons in time of flight scale, time-gating techniques can be applied. The total number of photons that arrive at the detector within a prescribed time window is measured.

Previously, the application of time-domain measurements for medical imaging has been used for time-gating to identify those photons that first emerged from the tissue which we assume to have traveled the shortest distance and therefore are the least scattered. This approach is, however, limited by the number of available photons with a sufficiently short time-of-flight. For instance, Hebden and Delpy et al showed that a degree of high-resolution information is encoded in the shaped end of the TPSF and can be extracted if the TPSF is measured accurately [16]. The time-gating techniques show that late arrival photons are predominantly affected by absorption; early arrival photons depend on both absorption and scattering of tissue.

Selb et al [31] showed that time-gating can be used to provide more depth resolution than CW measurements alone by rejecting light from tissues. Pulsed lasers are used as the light source for time-resolved measurements. The drawback of a time-domain system is that it requires an expensive pulsed laser source. Fast streak cameras or slow single-photon-counting detection systems are necessary. These detectors have a longer time to acquire data for a significant number of photon counts.

Time-resolved measurements of photons can distinguish between temporally correlated (measured signal) and uncorrelated (noise such as thermal noise and background light) events. Hillman, Deply, and Schmidt et al [28] showed that, by increasing integration time for time-resolved measurement, they can improve the signal-to-noise ratio. This is important because very few photons will travel all the way through large tissue thickness (~10cm). The time resolve technique is used for large volume tissues and for small volume measurements and topography. Due to the high cost of the instrumentation and the slow acquisition speed, they are well-suited for large volumes of tissue tomographic imaging.

2.3.3 Frequency Domain System

The first frequency-domain measurement of photon migration in biological tissues was reported by Lakowicz et al [26]. The frequency domain system uses a high-frequency (in the range of megahertz) intensity-modulated source that measures the amplitude and phase of the detected light at one or several modulation frequencies, as shown in figure 2.4. When the light source is intensity modulated, it generates a diffuse photon density wave in a medium that has optical phenomena such as reflection, refraction, interference, and diffraction. The photon density wave propagates through the tissue, a highly scattering medium. Its amplitude is attenuated and the phase is shifted relative to the incident source wave.

The phase delay and the amplitude attenuation relative to the source wave can be detected at the tissue surface by a PMT detector or a CCD camera. Comparison of the transmitted signal and the original signal gives information about the difference in phase between the two signals. In a frequency domain system, the amplitude and phase of the sinusoidal wave are measured using the homodyne technique or the heterodyne technique. The transport of the modulated beam is described as the propagation of diffuse photon density waves. Given the differing effects of absorption and scattering on phase and the difference between signal phase and amplitude, a frequency domain instrument offers the ability to separate absorption and scattering features and accurately determines the optical properties in the scattering medium. In principle, the time-domain signal and frequency domain signal are related by the Fourier transform. While time-resolved measurements have the advantage of acquiring information at all frequencies simultaneously, frequency-domain systems can employ light sources and detectors that are significantly less expensive than those required for time-resolved systems.

The chosen frequency governs the image resolution and the sensitivity of absorption and scattering coefficients. David Boas et al [29] showed that higher frequencies decrease the signal-to-noise ratio. Usually, the frequencies used are around 100MHz. The frequency domain system can measure phase and amplitude accurately with a high signal-to-noise ratio (SNR), which makes the system suitable for both breast cancer imaging and brain activation imaging. The measured signals have perturbations in amplitude attenuation and phase delay

that depend on the location, size, and optical contrast of heterogeneous within-tissue volume. By solving the diffusion equation, the optical properties of the tissue can be calculated with software such as MatLab and C, using image reconstruction algorithms.

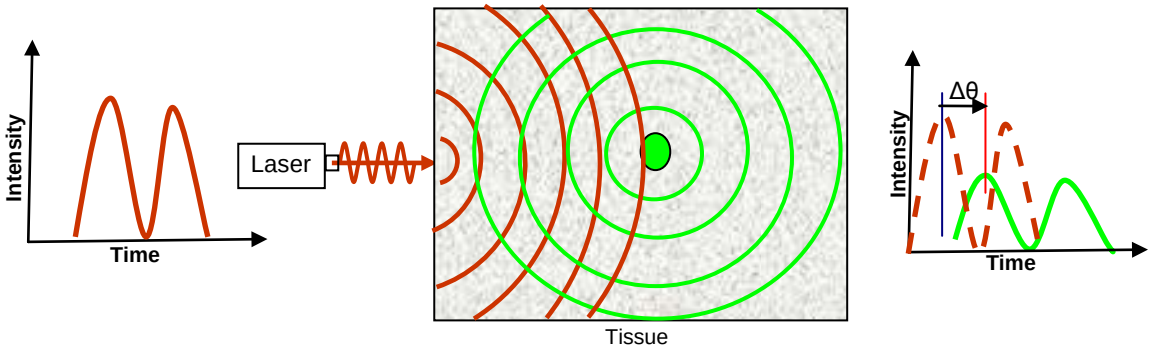

Figure 2.4: Schematic of a frequency domain method. The red line is incident intensity and the green line is detected intensity from the tissue. The phase difference between incident signal and detected signal is ΔΦ.

2.4 Fluorescent Diffuse Photon Density Wave

When light photons enter a scattering medium, the individual photons scatter many times and trace out random paths before exiting the medium. When the light source is sinusoidally intensity modulated, the propagation of light in the medium will produce a diffuse photon density wave. Macroscopically, the diffuse photon density develops and propagates spherically outwards from the source. Microscopically, the individual photons follow random walk-like trajectories. The

diffuse photon density wave has all properties of waves, although it is not a true wave, since energy is not associated with the wave.

The accurate model for photon migration in biological tissue is expressed by the radiative transport equation [33, 34]. Analytic solutions of the radiative transport equation are difficult to obtain and numerical calculations require large amounts of computational power. The solutions exist only for simple geometries, such as planar geometries and spherical geometries. For a highly scattering medium, the radiative transport equation can be simplified to the diffusion equation when the propagation of photons inside the tissue predominates by scattering. The diffusion equation is expressed as:

$$-D\nabla^2\phi(r,t)+\upsilon\mu_a\phi(r,t)+\frac{\partial\phi(r,t)}{\partial t}=\upsilon S_0(r,t)$$

where $\phi(r, t)$ is the photon fluence, $D=v\,[3\mu'_s]^{-1}$ is photon diffusion coefficient, μ_a is the absorption coefficient, μ'_s is the reduced scattering coefficient, and v is the velocity of light in medium. S_0 (r, t) is the source term.

The theoretical analysis of the fluorescent diffuse photon density wave requires localizing and characterizing the optical contrast of the inhomogeneities fluorophore embedded inside deep tissue. Two diffusion equations are used for a fluorescent diffuse photon density wave, one for excitation of the fluorophore and the other equation for the emission of the density wave from fluorophore. The equations are reduced to the Helmholtz equation. The photon influence is

calculated by applying boundary conditions of the born approximation to the Helmholtz equation.

2.5 Heterodyne and Homodyne Techniques

Frequency-domain optical tomography uses two different techniques for developing imaging systems for the diagnosis of cancer: the homodyne technique and the heterodyne technique. We have developed a fluorescent molecular tomography system based on a double super-heterodyne technique. The following section compares the homodyne technique and the heterodyne technique.

2.5.1 Homodyne Technique

The homodyne technique in frequency domain systems detects the phase shift at the radio frequency. The reference signal (local oscillator) is derived from the same source as the signal before the modulating process. The phase difference between the reference signal (local oscillator) and the signal pathway is detected. For instance, in laser scattering measurement, the laser beam is split into two parts. One is the local oscillator and other is sent to the tissue. The scattered light from the tissue is then mixed with the local oscillator in the detector. This technique has the advantage of being insensitive to fluctuations in the frequency of the laser. However, there is a lot of noise in the radio frequency. The signal-to-noise ratio is not high enough for phase detection. The basic circuit

of the homodyne system is explained by Ntziachristos V and Chance et al [30] briefly, figure 2.5 shows the homodyne system with a sine or cosine phase detector in a phase-quadrature (IQ) demodulator. The phase-shifted path involves a laser diode, an optical detector, an amplifier, and a narrow band filter. The output of the IQ detector is the sine and cosine components of the amplitude and phase.

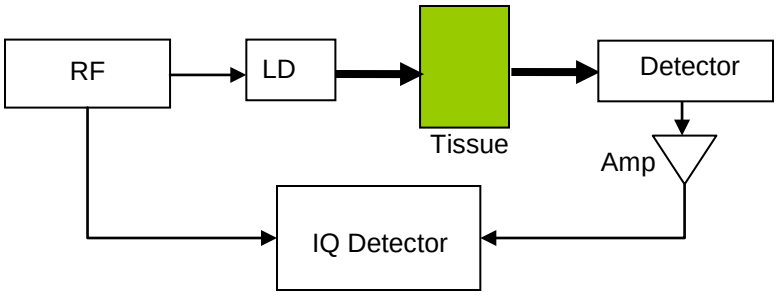

Figure 2.5: The schematic of homodyne detection system

2.5.2 Heterodyne Technique

For the heterodyne technique, the radio frequency signal (f_1) and the low frequency reference signal (f_2) (local oscillator) are superimposed at the mixer, which produces two different frequencies. One is the addition of frequencies; the other is the difference in frequencies, which form side-bands in the frequency domain system. Detecting one of the side-bands provides heterodyne detection. In our lab we use the super-heterodyne technique, as shown in the figure 2.6. The intermediate frequency is created by mixing the carrier modulated signal with

a local oscillator signal, resulting in a signal at the difference or beat frequency. An incoming signal is shifted to an intermediate frequency for the amplification before the final detection is done. For example, if the received signal is 5MHz and the local oscillator frequency is 4MHz, they are multiplied together, obtaining 1MHz and 9MHz frequencies. Usually the 1MHz is the Intermediate Frequency (IF). It is admitted (through a band pass filter) and later passed through the required electronic circuits for proper processing. In heterodyne detection, the high frequency components and usually the constant components are filtered out, leaving the intermediate frequency. The amplitude of intermediate frequency is proportional to the amplitude of the signal. The phase of incident frequency through the tissue or tissue-like phantoms gives the change in the phase and amplitude. Using the phase and amplitude information from the tissue and algorithms, the image reconstruction is done. Given the measurement with heterogeneous tissues and homogenous tissues (or phantoms), the differences in the phase and amplitude measured data can be used to obtain images that show the location of the changes in the optical properties of tissue.

2.6 Phase-Amplitude Cross Talk

Phase-amplitude cross talk is an important factor associated with the frequency-domain system to obtain stable and correct data. In order to get a large dynamic range of photon density from the tissue or phantom, the phase-

amplitude cross talk should be avoided [17, 18, 19]. The phase measurement depends on the average light intensity entering the detector.

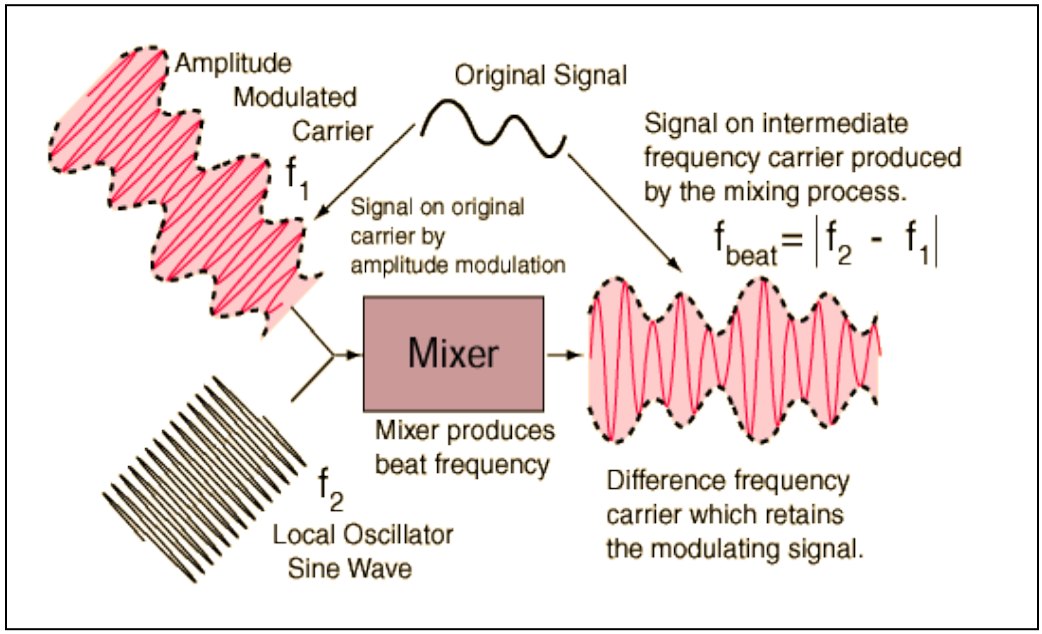

Figure 2.6: This figure represents the super-heterodyne technique. The intensity modulated signal f_1 and reference signal f_2 (local oscillator) are used to produce intermediate frequency f_2-f_1.

To study the phase-amplitude cross-talk we have built an experimental setup, as shown in figure 2.7. Briefly, we modulated the 144Mz radio frequency (RF) signal with a 2 kHz audio sinusoidal signal. The modulated signal is sent to the laser diode through the diode driver. The modulated optical signal is delivered through an optical fiber. A lens is used to collimate the light beam onto the sample (diffusing paper) filter; a wheel is used to select the different light

intensity entering the PMT-detector. A diffusing paper was placed in front of the detecting fiber bundle. We use the diffusing paper to simulate the photon diffusion process because the diffused photon should experience at least a single scattering. The intensity was first set to a low value and then was increased in discrete steps. The dependence of phase and amplitude was measured.

The light intensity in the PMT is controlled by the filter wheel to eliminate phase-amplitude cross talk. The different PMT-gain voltage plays an important role in producing good signal-to-noise ratio (SNR). We have studied different PMT gain voltages with different intensities. Briefly, figure 2.8 shows the phase as the function of different gain voltages. As shown in the figure 2.8A and 2.8B, the phase of the signal is not stable below 0.6mW for the gain voltages of 0.9 and 0.8. From figure 2.8C, the phase of the signal is not stable below 0.7mW for the gain voltages of 0.7 and 0.6. Those figures show a cutoff intensity of 0.6mW. Below this intensity, there is phase-amplitude cross talk. We have done phase measurements at the gain voltages of 0.5v and 0.4v. In this case, the noise in the signal is high.

With phase-amplitude cross talk, we have a chance of obtaining artifacts in the image reconstruction. In order to use the instrument for diagnostic imaging, we should avoid phase-amplitude cross talk. In our system, the source-detector distance is limited to 8cm; this distance can be increased by using a good modulation. We can obtain highly accurate measurements of the phase and amplitude only if the amplitude and phase of the signal is in a certain range. The upper limit is determined by the PMT-detector, where the anode is current and

the intensity is large enough before the phase-amplitude cross talk becomes significant. The lower limit is determined by the magnitude of leak of light between the source and detector and the RF interference. The instrument developed is used to measure the data with a high signal-to-noise ratio at close source-detector separations, making it useful for the detection of small changes in oxy- and de-oxy of hemoglobin. The system is suitable for tomographic imaging of small animal and breast cancer. An increase in PMT rise time with decreasing input average light intensity causes phase-amplitude cross talk. The graphs in figure 2.8 below show the phase as a function of incident intensity with different gain voltages of PMT. By changing the filter wheel, we are able to change incident intensity on the detector.

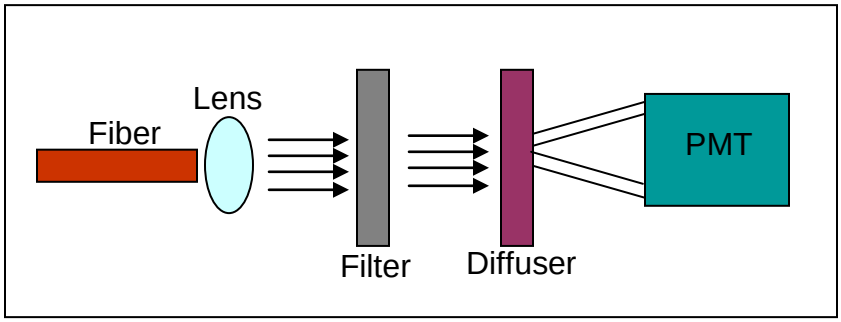

Figure 2.7: The experimental setup for the phase-amplitude cross-talk studies. Lens is used for collimation of light; the filter wheel is used for intensity change.

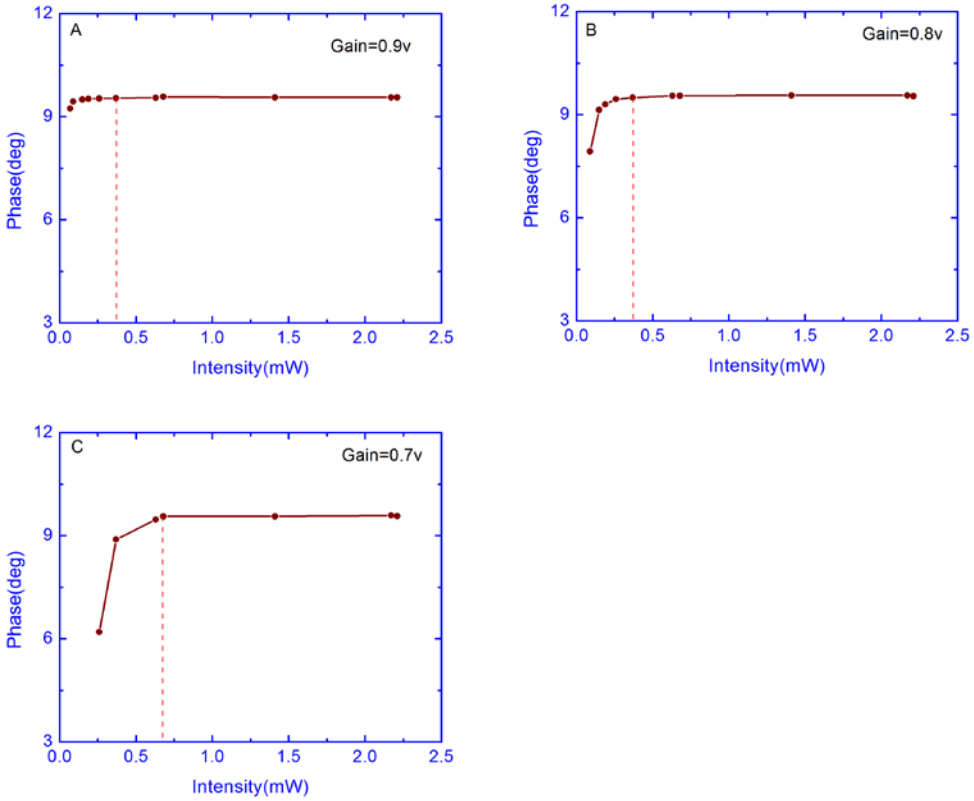

Figure 2.8: The phase as function of intensity of light entering the PMT-detector with different PMT gain voltages for phase-amplitude cross talk.

2.7 Radio Frequency Modulation Depth of Laser Diode

As described above, the phase information from the tissue in a frequency domain system can be used for tumor imaging. The high sensitivity of the phase detection is important for early detection of cancer cells. The modulation of the laser diode is important for determining the sensitivity of the system [20]. The photon density has two components: the AC component and DC component. The ratio of the AC component to the DC component of the diffuse photon density

wave is defined as the modulation. The AC component plays a critical role in the location of heterogeneous biological tissue in a volume of samples or phantoms. Biological tissue is a scattering medium. The AC component of the diffuse photon density wave decreases more rapidly with propagation through tissue than the DC component. We have studied the modulation with different currents of the laser diode to obtain the best modulation depth, so that the diffuse photon density wave can propagate deeply in the tissue and obtain accurate information at the detector. We have measured the RF modulation of the laser diode with different PMT gain voltages to examine which gain voltage is best in our system. The results are shown in figure 2.9. The red dotted line shows that we can achieve a maximum RF modulation of 70% with the DC current of the laser diode of 50mA. We were able to achieve an RF modulation depth at 70% in the range of 30mA to 50mA of the anode current of the laser diode with the PMT gain voltage of 0.9V.

2.8 Stability of Phase

The frequency domain fluorescent molecular tomography system is being developed using radio frequency (RF) modulation techniques. There is a chance of interference in the RF signals from the environmental RF signal. When this occurs, we will get false information about the phase and the heterogeneity in the tissue. To avoid the RF signal interference from environment, we have to make

sure that there is no leakage of the RF signal from the system. Figure 2.11 shows the phase stability of the fluorescent molecular tomography system.

Briefly, we have studied the stability of phase with four attenuations: 20dB, 40dB, 60dB and 80dB for 2 hr.

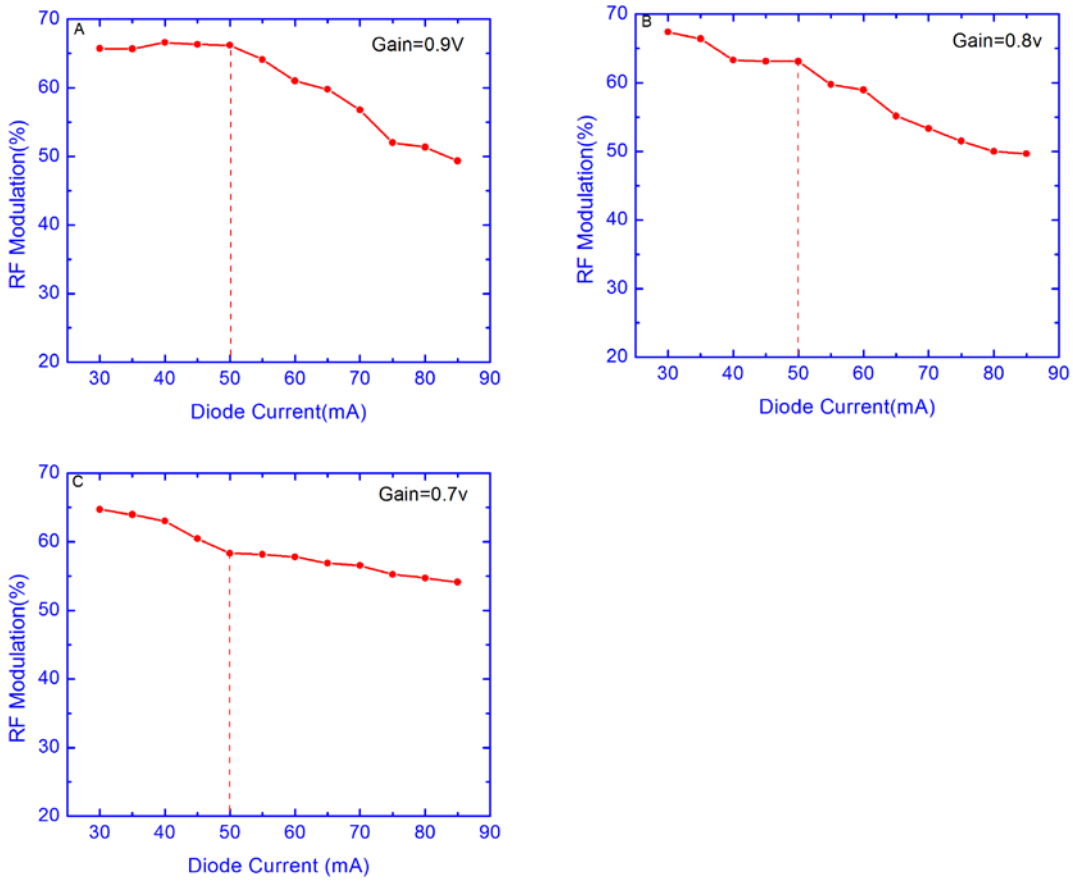

Figure 2.9: A, B, and C represent the radio frequency modulation with different gain voltage of PMT as a function of the Anode current of the laser diode. At a current of 50mA, the radio frequency modulation depth is 70% for gain voltages 0.9, 0.8, and 0.7

Each attenuator is connected across the transmitter and receiver with an RF frequency of 144.002MHz. The data is acquired using Labview software. The data is collected for 3 hours to study the phase stability in the system. For all different attenuations, the phase drift was 0.06º for 3 hours. In order to obtain a stable phase, we have placed devices and components in a 19-inch rack; the cable ends from the detector and receiver were covered with aluminum foil to avoid leakage of RF. Next, we studied phase stability with optical components in the system. The intensity wheel was kept in the laser beam to select a desired intensity. The experimental arrangement is shown in figure 2.10. The phase drift was 0.03 over 3 hours.

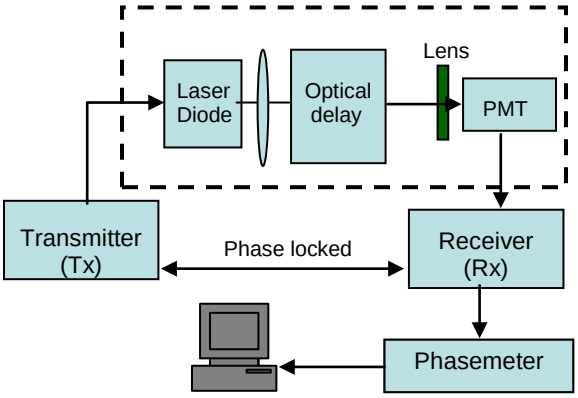

Fig A

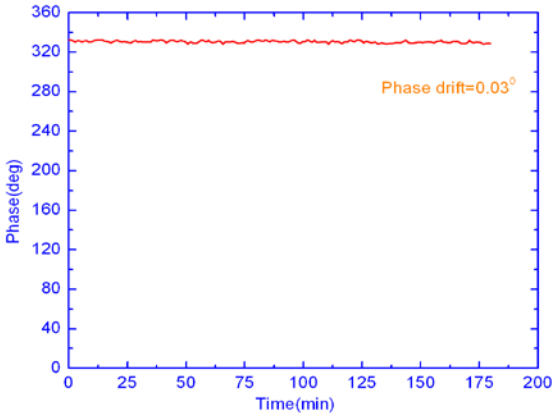

Fig B

Figure 2.10: The stability of system. (A) Represents the schematic diagram of FMT system with optics. (B) Represents phase drift as a function of time with optical components.

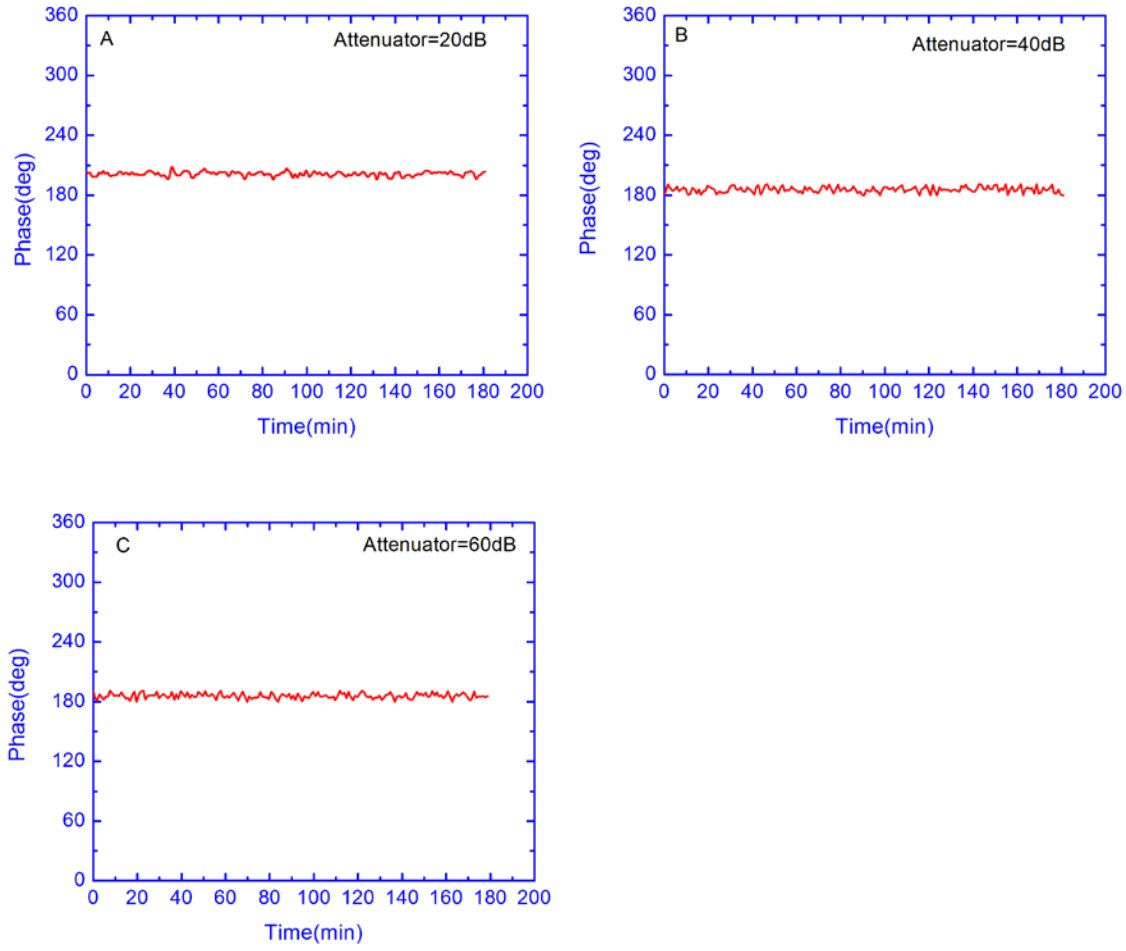

Figure 2.11: A, B, and C represent the stability of the phase with different attenuators as a function of time. The phase drift is 0.06° over 3 hours.

2.9 Experimental Setup

The FMT imaging system primarily consists of optical components, electrical components, and a data-acquisition software program. In this section, I will discuss the light source, radio frequency modulation, light detection, the design of the filter sets, and its hardware setup. Figure 2.12 represents the scheme of the FMT system. Our system works in a near-infrared wavelength as the photon propagates deeply through the tissue and provides a unique approach for molecular-based diagnostic imaging with near-infrared excitable fluorescent contrast agents that can be conveniently conjugated for targeting tumors.

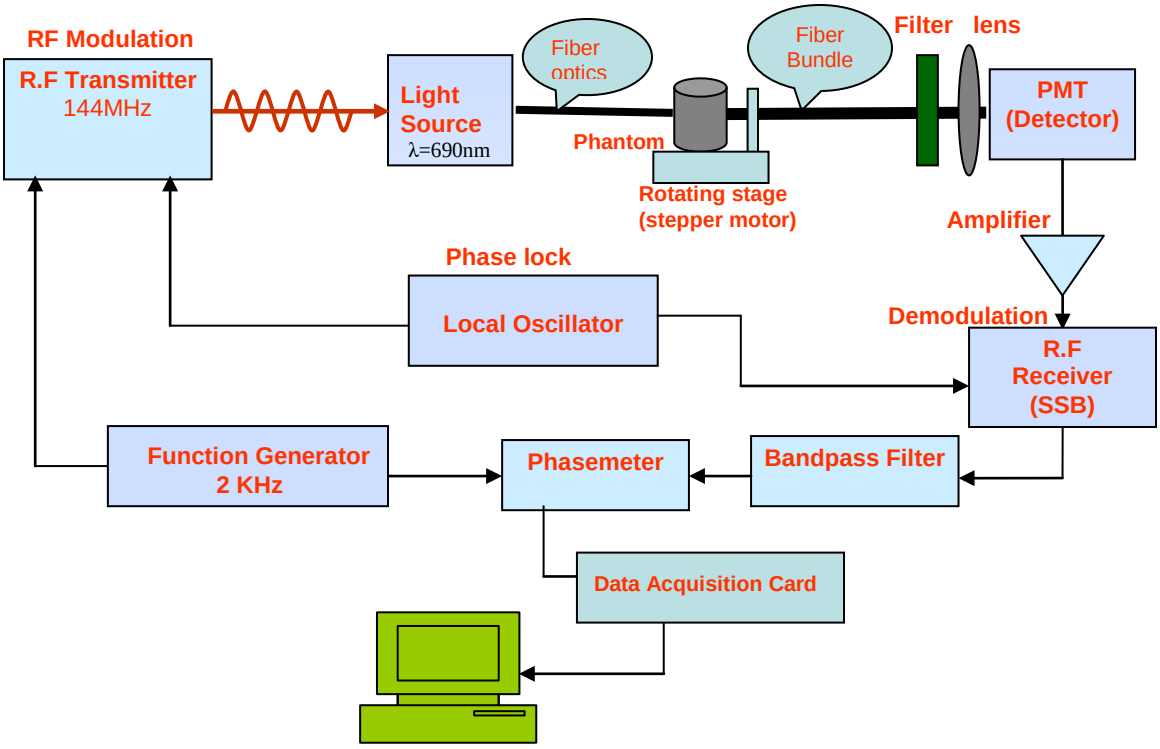

Figure 2.12: The scheme of FMT system.

We have developed a frequency domain fluorescent molecular tomographic system with single channel detection that enables us to measure molecular probes with the Alexa Fluor 680 and the Alexa Fluor 750. These fluorescent dye molecules are conjugated with Bombesin and have high binding affinity to the Gastrin Releasing Peptide receptor (GRPr) in T47-D human breast and PC-3 prostate cancerous cells. The system has a stable phase for a long time, high sensitivity, spatial resolution, penetration depth up to 8cm, and fast acquisition time for entire data sets with the Labview software program. The instrument we have developed can measure the phase and amplitude accurately (0.06º in phase) with a high signal-to-noise ratio at different intensities.

2.9.1 Light Source

The light source for the FMT system is a single-mode semiconductor AlGaInP laser diode (LD) with a multi-quantum well (MQW) structure. We purchased the Laser diode (HL6738MG) from Opnext Hitachi. The LD has a maximum output power of 35mW and a wavelength of 690nm. We use a TCLDM9 laser diode mount from Thorlabs, which is a temperature-controlled and radio frequency input using bias-tee that allows the laser to directly modulate up to 500MHz. We have used two wavelengths: 690nm for molecular probe Alexa Fluor 750 and the 830nm near infrared wavelength for cone phantom studies (we have borrowed cylindrical cone phantoms from University College of London, UK). The laser diode controller (LDC210 Thorlabs, inc.) is used to control the anode current of the laser diode in the laser diode mount; the thermoelectric

temperature controller (TED200 Thorlabs, Inc.) is set at 19.95°C in order to maintain the mode stability of the laser diode.

2.9.2 Radio-Frequency Modulation System

The FMT system in our lab uses the double-conversion Superheterodyne technique; the frequency of the RF is between 100MHz and 500MHz. The system consists of two units of transceivers of Yaesu FT-817ND operated in a single side band (SSB) with an upside band (USB) mode. The two units are phase locked with an external reference oscillator (TCXO-9) in order to synchronize the RF transmitter and the RF receiver to get the phase signal. An amplifier is connected to the reference oscillator (TCXO-9) to allow the driving power to operate the transmitter and receiver. A modulation frequency of 144MHz is used to study tissue phantoms. The function generator (Stanford Research Systems DS345) generates a sinusoidal signal at the frequency of 2kHz, which is used to modulate the intensity of the light source (Laser diode). The 144MHz RF signal is modulated with a 2kHz signal through the laser diode driver, using an SMA connecting point. The laser diode mount (TCLDM9 Thorlabs, Inc. NJ USA) couples the RF and DC currents through a Bias-Tee.

The 144.002MHz modulation frequency guided by the laser diode is transmitted to the tissue phantom through a multimode optic fiber. The laser source produces the source light at a wavelength of 690nm, with a maximum power of 20mW. The output power of the source light can be adjusted to a desired level by adjusting the anode current of the laser diode controller. The

sinusoidally intensity-modulated source light is labeled the AC light; the constant intensity light is the DC light. The AC light is guided into the fiber. In order to avoid RF signal interference, we have used RG 58/U and RG 174/U cables, which have good shielding for RF signal inference between the transmitter and the receiver in the FMT system.

2.9.3 Light Detection

We use the photomultiplier tube (PMT) as a detector to collect the fluorescent diffuse photon density wave from the tissue or phantom. The detector we use is the Hamamastu H6780-20 photosensor module, which consists of the R7400U-20 photomultiplier tube and a high-voltage power supply. The spectral response of the PMT is between 300nm and 900nm. The PMT detector has an input voltage of 11.5v to 15.5v. The maximum input voltage and current are 18v and 30mA respectively. The control voltage range is between 0.25v and 0.9v. The rise time is 0.78nsec. The ripple noise maximum (peak to peak) is 0.6v. The settling time is 0.2sec. Optical fibers are used to deliver the light to the surface of the phantom and a fiber bundle is used to collect the fluorescent photons onto the photocathode of the PMT. Fibers with a large numerical aperture have a wide acceptance angle for more fluorescent light photons from the phantom. We used a fiber bundle with an internal diameter of 2mm.

The fluorescent diffuse photons from the tissue phantom were collected by the fiber bundle and detected by the PMT (Hamamastu H780-20). In order to measure the fluorescence photons, a filter setup was kept in front of the PMT

detector. The collimator lens and longpass (LP) filter were used to allow only fluorescent diffuse photons from the tissue phantom to reach the PMT. The modulated signal from the PMT was delivered to a pre-amplifier to amplify the low signals. The amplified RF signal from the pre-amplifier was sent to the receiver in upper side band (USB). The receiver demodulated the 2kHz signal with a narrow-band single side band with upper side band mode and passed to the bandpass filter to eliminate the noise in the signal. The signal from the bandpass filter was sent to the phasemeter (Krohn-Hite, 6500A) for the detection of the phase signal. The phasemeter has two input channels: one is connected to the 2kHz function generator and other is connected to the bandpass filter. It compared the incoming signal and the function generator signal, which provided a phase shift between the signals. The resulting phase signal from the phasemeter was an analog signal. We used an interface to convert the analog signal to a digital signal. A 16-channel USB-data acquisition card from the National Instrument was connected to the computer from the interface. The data was acquired through Labview software. The drivers for the data acquisition card were downloaded from National Instrument.

The software can acquire data at a 1msec speed. The data was stored in an Excel spreadsheet. Figure 2.14 shows a picture of the FMT system. All the optical components and electrical components were placed in a 19” rack frame so that it could be easily moved to a hospital in the future.

2.9.4 Filter Set Design

A special design was made for the filter set in front of the PMT to collect the fluorescent diffuse photons from the phantom tissue. This is very important for the diffuse photon measurement, as the transmission properties of the thin film filter is dependent on the angle, as shown by Yu Chen et al [32]. As the angle of incidence increases, the transmission of the thin film on the filter shifts to shorter wavelengths. The fluorescent diffuse photon density wave coming from the fiber bundle is dependent on the thin film filter at various angles. This causes the leakage of the fluorescent signal. The leakage problem is overcome with the collimation of light using a convex lens in front of the PMT. Figure 2.13A and 2.13B show the design of the filter with the collimation lens. One end of mount has a diameter of 2.5cm, where the LP filter and lens can fixed in the mount. This end is connected to the PMT. The other end of the mount has a diameter of 1.5cm for fiber bundle to slide in the mount. The top of mount has screws for adjusting the focal plane of the lens.

We are using a long pass filter with a cutting wavelength 750nm and an optical density of 4. The mount was designed in such way that one end mounts with the fiber bundle and the other end mounts to the PMT. A convex lens is used to collimate the light on the long pass filter. A short focal length lens is used to focus the light on the PMT detector. The entire setup is enclosed to avoid any stray light entering the PMT.

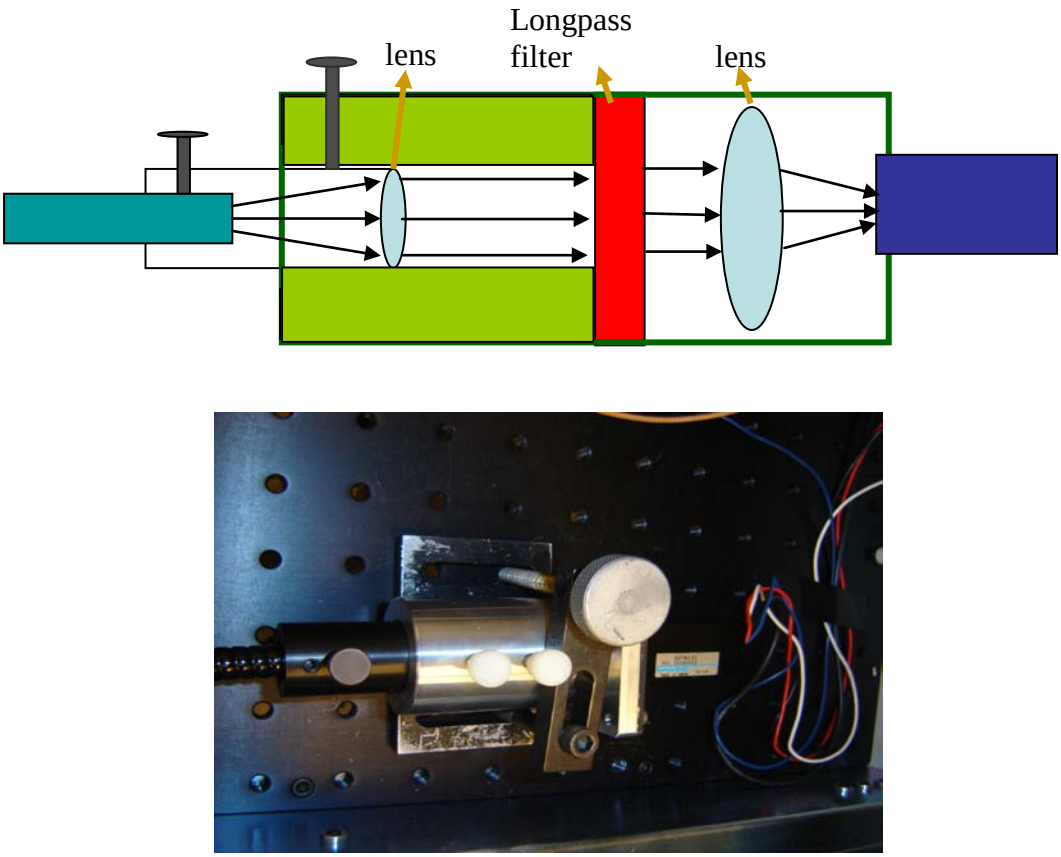

Figure 2.13: Figure represents the block diagram of the collimator with the long pass filter of wavelength 750nm and shows the arrangement in the experimental setup.

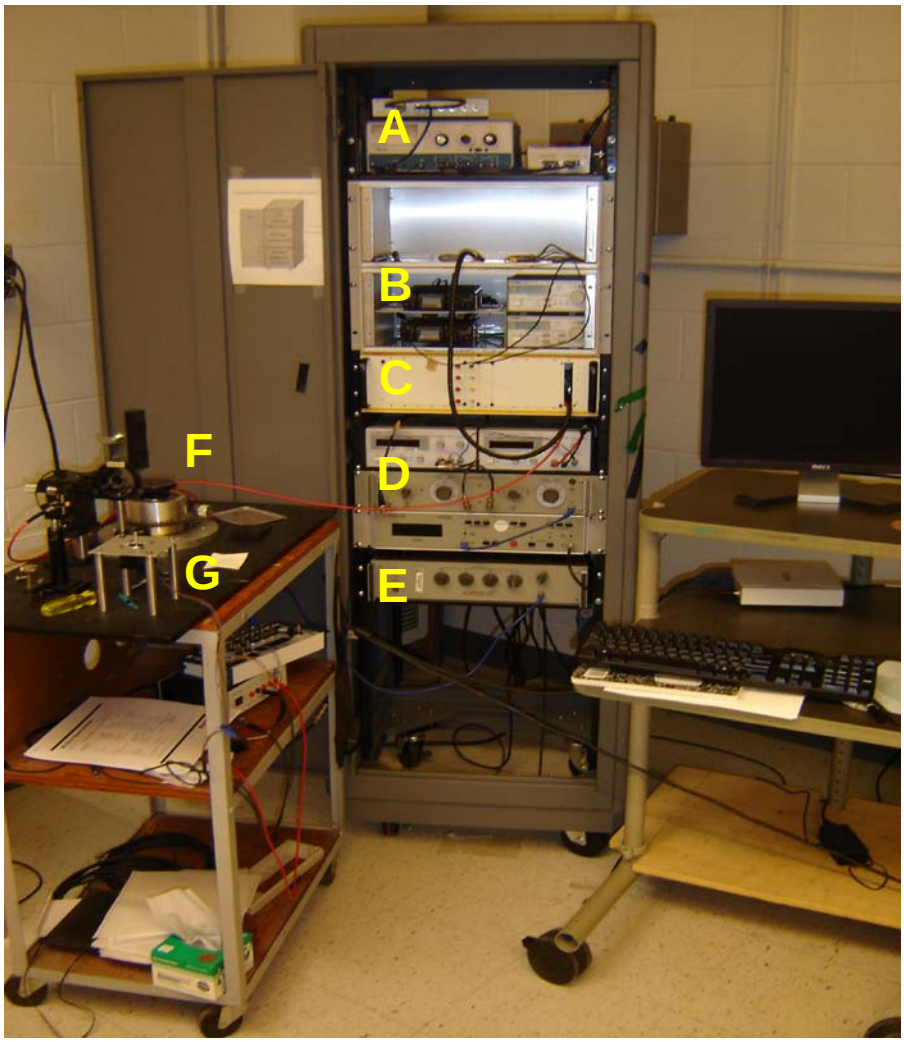

Figure 2.14: Picture of FMT system. A) Reference oscillator, B) Transmitter and Receiver, C) Laser diode mount and PMT (optical components), D) Voltage controller and gain controller for PMT, E) Phasemeter and bandpass filter, F) Fiber optics, and G) Stepper motor and stage.

2.10 Phantom Studies

To test the performance of the FMT system, two different phantom studies have been performed. We borrowed two conical breast phantom tissues from the University College of London (UK). One conical breast phantom tissue was homogenous and the other had three small cylinders with different optical properties. The transport scatter coefficient of the breast tissues was in the range of 0.6 to 1.3mm^{-1}. Overall, most evidence suggests that the ratio between the values of both the absorption coefficient and the reduced scattering coefficients for healthy and diseased tissues are of the order of a factor of 2. Briefly, the phantom tissues were made of titanium dioxide particles mixed with near infrared dye (ProJet NP900) for scattering and absorption of a diffuse photon density wave. This mixture was mixed with epoxy resin to form solid tissue phantoms with optical properties to reduce the scattering coefficient (μ_s') 0.8 $mm^{-1,}$ the absorption coefficient (μ_a) 0.007 $mm^{-1,}$ and the refractive index of 1.56. There were three cylinders with optical properties of 2 μ_s' and μ_a: μ_s' and 2μ_a: 2 μ_s' and 2μ_a in the second conical breast phantom. These three cylinders, with a height of 10mm, were located in a single plane equidistant from the central axis. The bottom diameter of the conical phantom was 135mm and the height was 122mm. The upper portion of the 50mm phantom is cylindrical; the lower portion of the 72mm phantom was conical.

The data acquisition for the phantom was performed using Labview software. Figure 2.15A and 2.15B shows the experimental arrangement of the conical phantom and the data acquisition of the phase as a function of the

detector position around the conical phantom. The modulated RF signal from the laser diode was sent to the optic fiber, which delivers the modulated intensity signal to the surface of the conical tissue phantom. The diffuse photon from the phantom is collected by the fiber bundle, which is connected to the PMT for the detection of diffuse photons from the phantom. The fiber bundle is moved around the tissue phantom for 16 positions and each position is separated by 2cm. The collected signal intensity from the PMT is plotted as function of the position of the detector, as shown in figure 2.15B. The phase is decreasing when the fiber bundle is moved 180° and then it is increasing.

Further studies have been performed with several handcrafted phantoms. Figure 2.16 shows the results of a handcrafted phantom for phase changes with the position of detector. Briefly, three tubes with a molecular probe AF750 with saline solution were filled and placed in the turbid medium (milk solution) with a length of 6cm. We use a saline solution to match the refractive index of tissue. The same method was repeated, as described above. The modulated signal was delivered to the phantom surface through the optic fiber and the fiber bundle was used to collect the diffuse photons from the phantom surface. Figure 2.16B shows the phase as a function of detector positions. The presence of AF750 conjugate causes the change in phase of the signal. From two different phantoms, we can show that our system is very sensitive to heterogeneity in tissue volume. We can measure both the phase and the amplitude signal of the fluorescent diffuse photons from the tissue surface. We further developed a system for the detection of molecular probe AF750 conjugated with bombesin for

small animal imaging to study prostate and breast cancer with magnetic resonance imaging. The system allows the light to penetrate several centimeters into the medium before being absorbed or scattered through boundaries. Therefore, it can be used for breast, brain, and skeletal muscle.

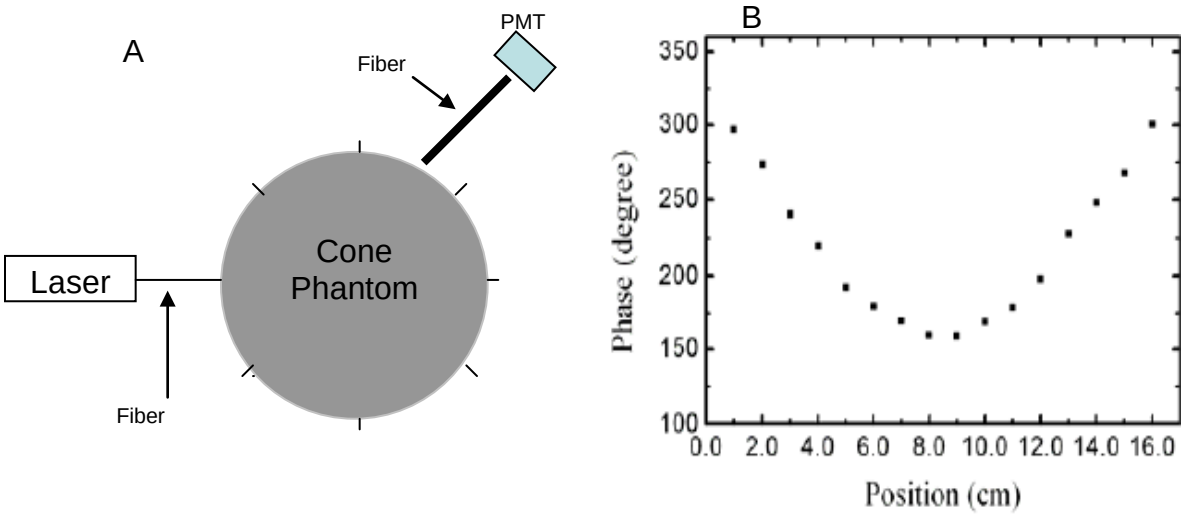

Figure 2.15: Figure A: represents an experimental view of collecting data from conical phantom with source fiber is fixed and fiber bundle is moved to different positions. Figure B: represents the data acquisition of phase as a function of position of detector.

.

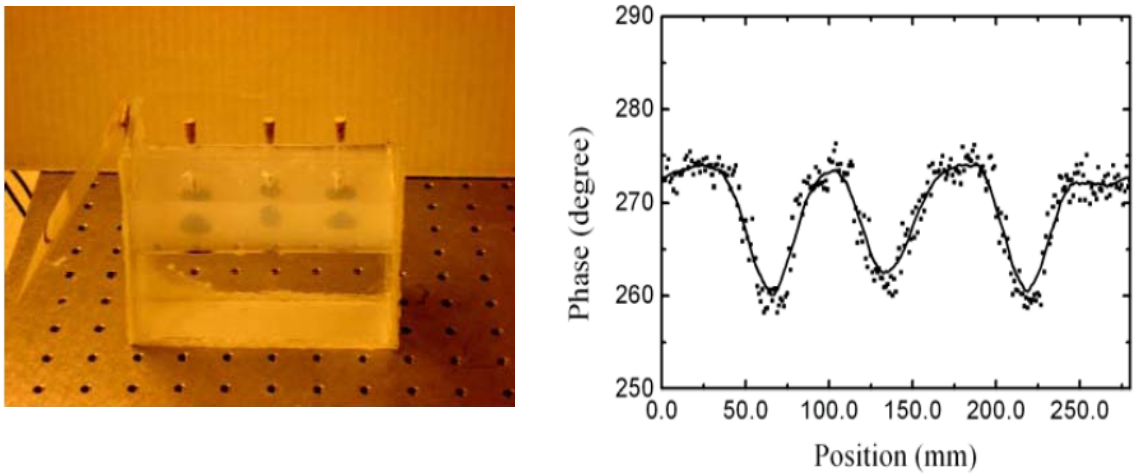

Figure 2.16: Figure A represents the three tubes with different concentrations of molecular probe AF 680. Figure B represents the phase as function of position of detector.

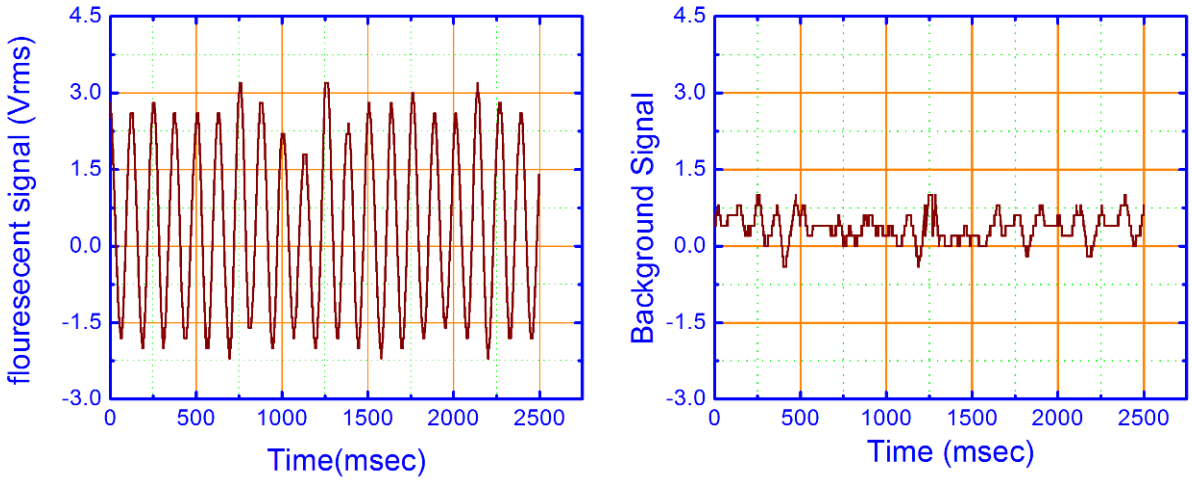

Figure 2.17: The graphs of RMS voltage of fluorescent signal and background signal from Alexa Fluor 750-bombesin.

Studies have done to determine the fluorescent signal intensity from the AF-750 bombesin conjugate (Fluorescent probe). The fluorescent probe in distilled water with 1:10 is placed in the quilt tube with the same experimental methods described in the previous section to study the fluorescent signal intensity from the probe. The SNR is calculated for the fluorophore. We achieved a signal-to-noise ratio of 18.4dB, which is an indication of a very good fluorescent signal (figure 2.17). The SNR value tells us what amount of fluorophore is necessary to prepare phantom studies.

Bibliography:

1. Chance B. “Oxygen transport to tissue XV”. Plenum Press, New York, (1994)
2. Ishimaru A. “Diffusion of light in turbid media”. Appl. Opt, Vol. 28, 2210-2215 (1989)
3. Jobsis FF. “Noninvasive, infrared monitoring of cerebral and myocardial oxygen sufficiency and circulatory parameters”. Science, Vol.198, 1264-1267 (1977)
4. Cope M. “The application of near infrared spectroscopy to non-invasive monitoring of cerebral oxygenation in the newborn infant”. PhD Thesis, University College London, Department of Medical Physics and Bioengineering, London (1991)
5. Godavarty A, Thompson AB, Roy R, Gurfinkel M, Eppstein MJ, Zhang C and Sevick-Muraca EM. “Diagnostic imaging of breast cancer using fluorescence-enhanced optical tomography”. Biomedical Optics, Vol. 22, 345-360 (2004)
6. Ntziachristos V and Weissleder R. “Experimental three-dimensional fluorescence reconstruction of diffuse media by use of normalized born approximation”. Optics Letter, Vol. 26(12), 893-895 (2001)
7. Tarvainen T, Vauhkonen M, Kolehmainen V, and Kaipio JP. “Hybrid radiative-transfer diffusion model for optical tomography”. Applied Optics, Vol. 44(6), 876-880 (2005)

8. Achilefu S, Dorshow RB, Bugaj JE and Rajogopalan R. “Novel receptor-targeted fluorescent contrast agents for in vivo tumor targeting”. Investig. Radiol, Vol. 35, 479-485 (2000)
9. Becker A, Hessenius C, Licha K, Ebert B, Sukowski U, Senmler W, Wiedenmam B and Grotzinger C. “Receptor-targeted optical imaging of tumors with near-infrared fluorescent ligands”. Nat. Biotechnol, Vol.19, 327-331 (2001)
10. Zaheer A, Lenkinski RE, Mahmood A, Jones AG, Cantley LC and Frangioni JV. “In vivo near-infrared fluorescence imaging of osteoblastic activity”. Nat. Biotechnol, Vol. 19, 1148-1154 (2001)
11. Oleg AA, Dupuy AD, Michael Segele, Srikanth Sandugu, David A Serra, Clinton O Chichester, Donald M Engelman and Yana K Reshetnyak. “Mechanism and uses of a membrane peptide that targets tumors and other acidic tissues in vivo”. PNAS, Vol. 104(19), 7893-7898 (2007)
12. Arridge SR. “Photon measurement density functions. Part I: Analytical forms”. Applied Optics, Vol.34, 7395-7409 (1995)
13. Arridge SR and M Schweiger. “Photon measurement density functions. Part II: Finite element method calculations”. Applied Optics, Vol. 34, 8026-8037 (1995)
14. Arridge SR and Lionheart WRB. “Nonuniqueness in diffusion-based optical tomography”. Optics Letter, Vol. 23, 882-884 (1998)
15. Hebden JC, Arridge SR, and Delpy DT. “Optical imaging in medicine: Experimental techniques”. Phys. Med. Biol, Vol. 42(5), 825-840 (1997)

16. Hebden JC and Delpy DT. “Enhanced time resolved imaging using a diffusion model of photon transport”. Optics Letter, Vol.19, 311-313 (1994)
17. Nissila I, Kotilahti K, Fallstrom K and Katila T. “Instrumentation for the accurate measurement of phase and amplitude in optical tomography”. Rev. Sci. Inst, Vol. 73(9), 3306-3312 (2002)
18. Nissila I, Noponen T, Kotilahti K, and Katila T. “Instrumentation and calibration methods for the multichannel measurement of phase and amplitude in optical tomography”. Rev. Sci. Inst, Vol. 76, 044302 (2005)
19. Hillman E, Hebden JC, Florian Schmidt, Arridge SR, Martin Schweiger, Hamid Dehghani, and Delpy DT. “Calibration techniques and datatype extraction for time-resolved optical tomography”. Rev. Sci. Inst, Vol. 71(9), 3415-3427 (2000)
20. Li X, Chance B, and Yodh AG, “Fluorescent heterogeneities in turbid media: limits for detection, characterization, and comparison with absorption”. Appl. Opt, Vol. 37, 6833-6844 (1998)
21. Achilefu S, Dorshow RB, Bugaj JE and Rajogopalan R. “Novel receptor-targeted fluorescent contrast agents for in vivo tumor targeting”. Investig. Radiol, Vol. 35, 479-485 (2000)
22. Becker A, Hessenius C, Licha K, Ebert B, Sukowski U, Senmler W, Wiedenmam B and Grotzinger C. “Receptor-targeted optical imaging of tumors with near-infrared fluorescent ligands”. Nat. Biotechnol, Vol. 19, 327-331 (2001)

23. Zaheer A, Lenkinski RE, Mahmood A, Jones AG, Cantley LC and Frangioni JV. “In vivo near-infrared fluorescence imaging of osteoblastic activity”. Nat. Biotechnol, Vol. 19, 1148-1154 (2001)
24. Reshetnayak YK, Andreev OA, Segala M, Markin VS, Engelman DM. “Enegetics of peptide (pHLIP) binding to and folding across a lipid bilayer membrane”. PNAS, Vol. 105(40) 15340-5 (2008)
25. Elizabeth Hillman: “Experimental and theoretical investigations of near infrared tomographic imaging methods and clinical applications”. PhD Thesis, University College of London, Department of Medical Physics and Bioengineering, London U.K.
26. Lakowicz JR, Szmacinski H, Nowaczyk K, Berndt K, Johnson ML. “Fluorescence lifetime imaging”. Analytical Biochemistry, Vol. 202, 316-330 (1992)
27. Barbour RL, Graber HL, Pei Y, Zhong S, Schmitz CH. “Optical tomographic imaging of dynamic features of dense-scattering media”. J Opt Soc Am, Vol. 18(12), 3018-3036 (2001)
28. Hillman EMC, Hebden JC, Schmidt FEW, Arridge SR, Schweiger M, Dehghani H, Delpy DT. “Calibration techniques and datatype extraction for time-resolved optical tomography”. Rev Sci Instrum, Vol. 17(9), 3415-3427 (2000)
29. David Boas: “Diffuse photon probes of structural and dynamical properties of turbid media: theory and biomedical applications”. PhD

thesis, University of Pennsylvania, Department of Physics and Astronomy, Pennsylvania.

30. Ntziachristos V, Leary M, Chance G, Yodh AG. “Advances in optical imaging and photon migration”. Optical Society of America, Vol. 2, 164-168 (1996)
31. Selb J, Dale AM, Boas DA. “Linear 3D reconstruction of time-domain diffuse optical imaging differential data: improved depth localization and lateral resolution”. Optics Express, Vol. 15(25), 16400-12 (2007)
32. Yu Chen: “Contrast enhancement for diffuse optical spectroscopy and imaging: Phase cancellation and targeted fluorescence in cancer detection”. PhD thesis, Bioengineering, University of Pennsylvania (2003)
33. Ben A. Brooksby: “Combining near infrared tomography and magnetic resonance imaging to improve breast tissue chromophore and scattering assessment”. PhD thesis, Thayer School of Engineering, Dartmouth College, Hanover, New Hampshire, (2005)
34. Amit Joshi: “Adaptive finite element based frequency domain fluorescence enhanced optical tomography”. PhD thesis, Texas A & M University, Texas (2005)

Chapter 3

Molecular Probes Development

3.1 Introduction

Optical molecular imaging is an emerging technology in biology and medicine that can revolutionize our understanding of the treatment of cancers such as prostate and breast cancers. Optical molecular imaging may lead to a better means of differentiating tumors for earlier detection of disease and monitoring of therapies, using fluorescence molecules.

In recent years significant progress has been made in understanding the fundamental nature of light propagation in tissue, which has led to the development of several advanced techniques for migration of light through tissue. Optical molecular imaging provides distinctly new diagnostic capabilities and complements conventional imaging modalities such as MRI, CT, SPECT, and PET [1, 2, 3, 4]. The advantages of using optical techniques in biomedical imaging include non-ionizing radiation. It is non-invasive and has the capability of continuous data acquisition for real-time monitoring. It also has the potential for low cost portable imaging [5, 6].

This chapter describes the development of receptor-specific molecular probes for optical molecular imaging of prostate and breast tumors. We have developed molecular probes that demonstrate absorption and fluorescence in the near infrared wavelengths and specifically target prostate and breast cancer

cells. Initially, we performed research with Alexa Fluor 680 conjugated to a bombesin peptide using *in vitro* and *in vivo* methods [7, 8, 9]. The conjugate has shown high binding affinity and internalization to cancer cells. Further studies were performed with Alexa Fluor 750 conjugate because the migration of light in tissue is wavelength-dependent and NIR light has less absorption inside the tissue. In the 680nm wavelength region, numerous endogenous chromophores absorb light and emit auto-fluorescence. In the NIR region, absorption by intrinsic photoactive biomolecules is low, allowing light to penetrate several centimeters through tissues. This is useful for imaging prostate and breast cancer embedded in deep biological tissue and for the detection of early stages of cancer.

3.2 The Basic Physics of the Fluorescence Technique

The fluorescence output of a given dye depends on the efficiency with which it absorbs and emits photons and its ability to undergo repeated excitation/emission cycles. Absorption and emission efficiencies are most usefully quantified in terms of the molar extinction coefficient for absorption and quantum yield for fluorescence. The value of the extinction coefficient is specified at a single wavelength (usually the absorption maximum), whereas the quantum yield is a measure of total photon emission over the entire fluorescence spectral profile. The fluorescence intensity per dye molecule is proportional to the product of the molar extinction coefficient for absorption and the quantum yield. Below I briefly outline the fluorescence technique.

3.2.1 The Fluorescence Process

The fluorescence process is the result of a three-stage process that occurs in certain molecules (generally polyaromatic hydrocarbons or heterocycles) called fluorophores or fluorescent dyes. The fluorescence process involves fluorophore excited with the excitation wavelength and fluorophore emitted by a longer wavelength, the incident wavelength. . A fluorescent probe is a fluorophore designed to localize within a specific region of a biological specimen or to respond a specific stimulus. The process responsible for the fluorescence of fluorescent probes and other fluorophores is illustrated by the simple electronic-state diagram [11] (Jablonski diagram).

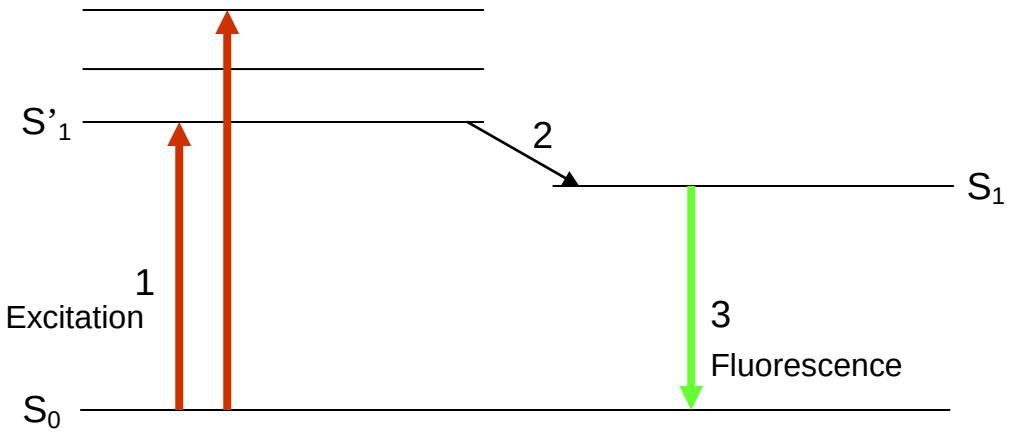

Figure 3.1: Jablonski diagram illustrating the processes involved in the creation of an excited electronic singlet state by optical absorption and subsequent emission of fluorescence. (1) Excitation, (2) Excited-state lifetime, and (3) Fluorescence emission

Excitation

A photon of energy (hv_{EX}) is supplied by an external source such as a laser source that is absorbed by the fluorophore, creating an excited electron in an excited electronic singlet state (S_1'). This process distinguishes fluorescence from chemiluminescence's, in which the excited state is populated by a chemical reaction. Similarly, the absorption process of fluorophore can provide a photon being absorbed in the same energy. The absorption band should be at the same wavelength as the excited band.

Excited-State Lifetime

The excited state exists for a finite time (typically 1-10 nanoseconds). During this time, fluorophore undergoes conformational changes and is subject to a multitude of possible interactions with its molecular environment. These processes have two important consequences. First, the energy of S_1' is partially dissipated, yielding a relaxed singlet excited state (S_1) from which the fluorescence emission originates. Second, not all the molecules initially excited by absorption return to the ground state (S_0) by fluorescence emission. Other processes such as collisional quenching, fluorescence resonance energy transfer (FRET) and intersystem crossing may also depopulate S_1. The fluorescence quantum yield, which is the ratio of the number of fluorescence photons emitted to number of photons absorbed, is a measure of the relative extent to which these processes occur.

Fluorescence Emission

A photon of energy hv_{EM} is emitted, returning the fluorophore to its ground state S_0. Due to energy dissipation during the excited-state lifetime, the energy of this photon is lower. Therefore the emission band has a longer wavelength than the wavelength of the excitation photon. The difference in energy or wavelength represented by hv_{EX}– hv_{EM} is called the Stokes shift. The Stokes shift allows emitted photons to be detected against a low background, isolated from the excited photons. By contrast, the absorption spectrum requires a measurement of transmitted light relative to incident light levels at the same wavelength.

3.2.2 Fluorescent Contrast Agent for Optical Molecular Imaging

The use of optical molecular (fluorescent) probes can fall into three categories: (1) Detecting early stage tumors, (2) differentiating benign from malignant tumors, and (3) monitoring and staging the status of cancer progression. Although numerous imaging modalities have been developed for visualizing pathologic conditions, the high sensitivity and relatively low energy radiation of the optical imaging method makes it attractive for optical molecular imaging [10].

This study focused on a family of NIR Fluorescence Alexa Fluor dye. Fluorescent molecules were utilized to enhance the tumor-to-normal contrast for increased sensitivity and specificity. For the fluorescence contrast, we used the Alexa Fluor dyes as the fluorescent molecule with fluorescence emission in the NIR spectrum. Fluorescent probes can detect particular components of complex

biomolecular assemblies, including living cells, with exquisite sensitivity and selectivity. The development of non-invasive diagnostic strategies for specific human cancers is a new and exciting approach for diagnosis and monitoring the progression of disease. Target identification and validation with high affinity through optical molecular probes is one of the key prerequisites for interrogation of specific molecular targets in prostate and breast cancer tumors. A high affinity probe that can bind tumors must have the ability to reach the specific target vector at sufficient concentration and for a sufficient length of time. The barriers of non-specific binding, rapid excretion, metabolism, and delivery must be overcome.

The Gastrin releasing peptide (GRP) receptors are over-expressed on several types of human cancer cells, including breast, prostate, small cell lung, and pancreatic cancers. GRP is the mammalian counterpart of bombesin (BBN). BBN is a 14 amino acid peptide that is analogous to that human gastrin releasing peptide that binds to GRPr with very high affinity and specificity, as shown in figure 3.2. GRP and BBN share amidated C terminus sequence homology of 7 amino acids. Furthermore, each of these peptides functions as gastrointestinal hormones and neurotransmitters, exerting a variety of physiological and pharmacological effects in various human systems. The performance of NIR fluorescent imaging is extremely good with sensitivity linearly related to the administered fluorophore concentration. NIR fluorescent contrast dye can bind to a target vector for specific tumor tissue. Therefore, the design and development of new site-directed, fluorescent targeting vectors for dynamic optical molecular

imaging of human prostate and breast cancers is significant. We have developed a conjugate of bombesin with an N-terminal fluorescent tag that is useful in diagnosis and assessing the progression of estrogen receptor positive breast cancer.

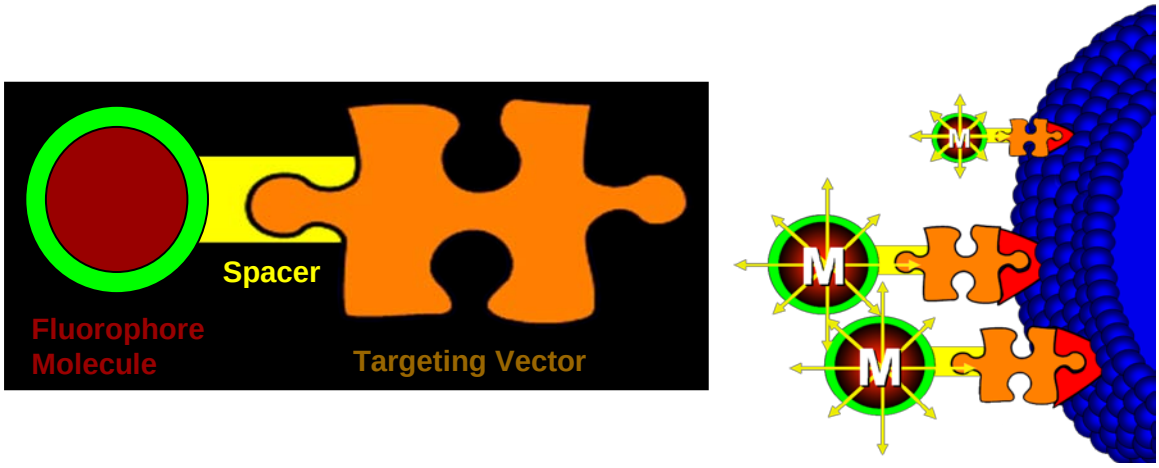

Figure 3.2: **Targeting Vector:** A peptide, protein, antibody or antibody fragment with high specificity and affinity for particular over-expressed receptors. **Spacer:** Inert chemical group that allows for fine-tuning of pharmacokinetic properties of the bioconjugate. **Alexa Fluor 750:** The NIR fluorophore. With fluorescent spectrum of excitation wavelength: 630nm-800nm, the excitation peak is 748nm and emission wavelength: 750nm-830nm, the emission peak is 778nm (Courtesy of: Dr. Ma, Adam P, Dr. Jeff Smith)

3.3 Conjugation Process and Fluorescence Spectrum of Probes

Below I describe the synthesis of the fluorescent probe for conjugation and characterization of the Alexa Fluor 750 and Alexa Fluor 680 dye with bombesin peptide for molecular imaging of prostate and breast cancer tissue. Fluorescence spectrum studies showed the fluorescent dyes maintain their optical properties for *in vitro* studies and *in vivo* studies.

3.3.1 The Process of Preparation of Optical Molecular Probe

The conjugation, purification, and analysis of Alexa Fluor 680 and Alexa Fluor 750 with bombesin peptide were conducted in the lab of Professor Jeff Smith. Peptide synthesis was performed on an applied biosynthesis model 432 automated peptide synthesizer, employing traditional Fmoc Chemistry. The reaction of HBTU activated carboxyl groups on the reactant with the N-terminal amino groups on the growing peptide provided a way for the addition of amino acid. The purification of a crude peptide was done by high performance liquid chromatography (HPLC) and the solvents were removed with the LABCONCO centriVap concentrator. For conjugation, approximately 2mg of stock solution peptide was added to 2.5mg of Alexa Fluor 750 succinimidyl ester in 250mL of dimethylformamide, with stirring. The purified peptide conjugation was obtained around ~60%, based upon reversed phase-HPLC (RP-HPLC). The HPLC analysis and purification of the peptide conjugate was performed on Waters 600s controller equipped with a 626 pump and 2487 dual wavelength absorption detector, the Eppendorf CH-30 column heater, and the Hewlett-Packard HP3395

integrators. Electrospray-ionization mass spectral (ESI-MS) was used to characterize the new Alexa Fluor 750-BBN[7-14]NH_2 peptide conjugate at the Proteomics Center biomolecular research facilities.

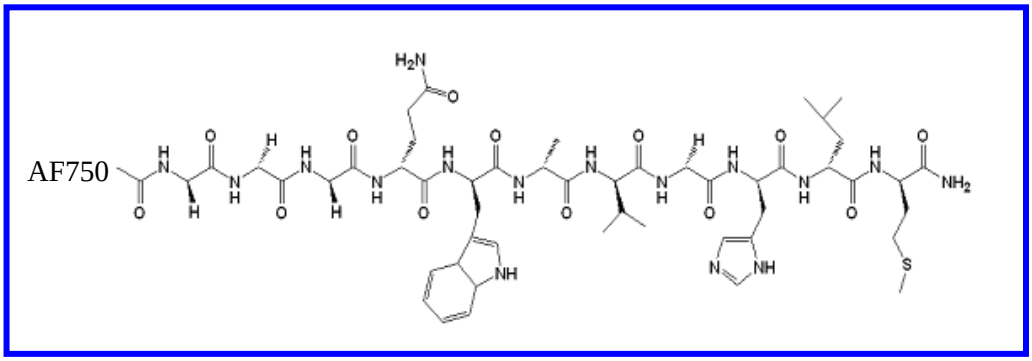

Figure 3.3: The molecular structure of optical molecular probe (AF750-βAla BBN[7-14]NH_2 Conjugate).

3.3.2 Absorption and Fluorescent Characteristics

The near-infrared fluorescence imaging is based on the absorption and emission of light with a wavelength between 700nm and 1000nm. The absorbed light excites a fluorescent molecule within the biological tumor tissue, which emits light (fluorescent emission) at a wavelength longer than the transmitted light. In the near-infrared range, biological tissue is not very fluorescent, but some tissues like stomach, kidney, bladder and small intestine do exhibit a degree of autofluorescence, which can reduce the signal-to-background ratio of the fluorescence image. However, autofluorescence can be removed by the appropriate choice of NIR filter sets. Studies of absorption and fluorescence of

optical molecular probe are performed exactly in the same way as described in Balasubramnanian et al [9]. Figure 3.4 indicates the absorption peak is at 679nm and the fluorescence emission peak is at 702nm for Alexa Fluor 680 conjugated with bombesin peptide. The excitation curve is acquired when the detection wavelength is set to 710nm. The spectrum was acquired with concentrations of 10:1 distilled water and Alexa Fluor dye, and then the spectrum was performed with an excited wavelength of 680nm and emission obtained at 702nm. The extinction coefficient is 184,000 and spectrally similar to Cy5.5dye, allophycocyanin (APC). The reactive dye used was Succinimidyl ester.

The spectrum of Alexa Fluor 680 bombesin fluorescent probe was acquired by using the spectrofluorometer RF-5301PC (SHIMADZU). The spectrofluorometer has two monochromators, before and after the sample chamber and is operated in the emission mode and excitation mode. In the emission mode, the exciting wavelength is fixed and the emission spectrometer is scanned over a given wavelength range. The synchronous scanning mode allows mixtures of fluorochromes to be analyzed. The high throughput optical system employs a blazed holographic grating and digital signal processing to provide the highest level signal-to-noise ratio. In the excitation mode, the emission spectrometer is fixed with a wavelength at the peak of the fluorescence spectrum and the excitation spectrometer is scanned over the desired wavelength range. The spectrum of the Alexa Fluor 680-GGG Bombesin [7-14]NH_2 conjugate is collected and the graph of the excitation and emission is plotted using Origin software. To study the fluorescence spectrum of the near-

infrared optical molecular probe Alexa Fluor 750-bombesin, I have used the ocean optics spectrometer. As seen in figure 3.5 the conjugate is excited with a wavelength of 693nm and the emission peak was obtained at 783nm.

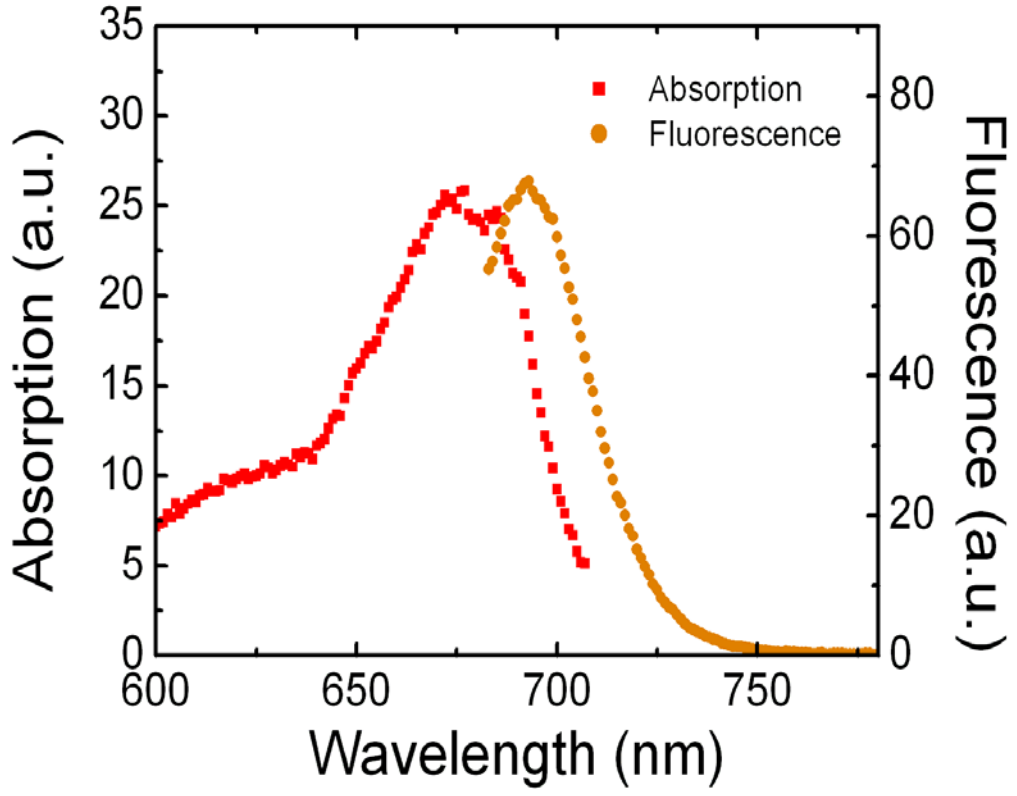

Figure 3.4: Spectra indicating the absorption and fluorescence of the Alexa Fluor 680-G-G-G-BBN[7-14] NH_2 Conjugate (Ref.9)

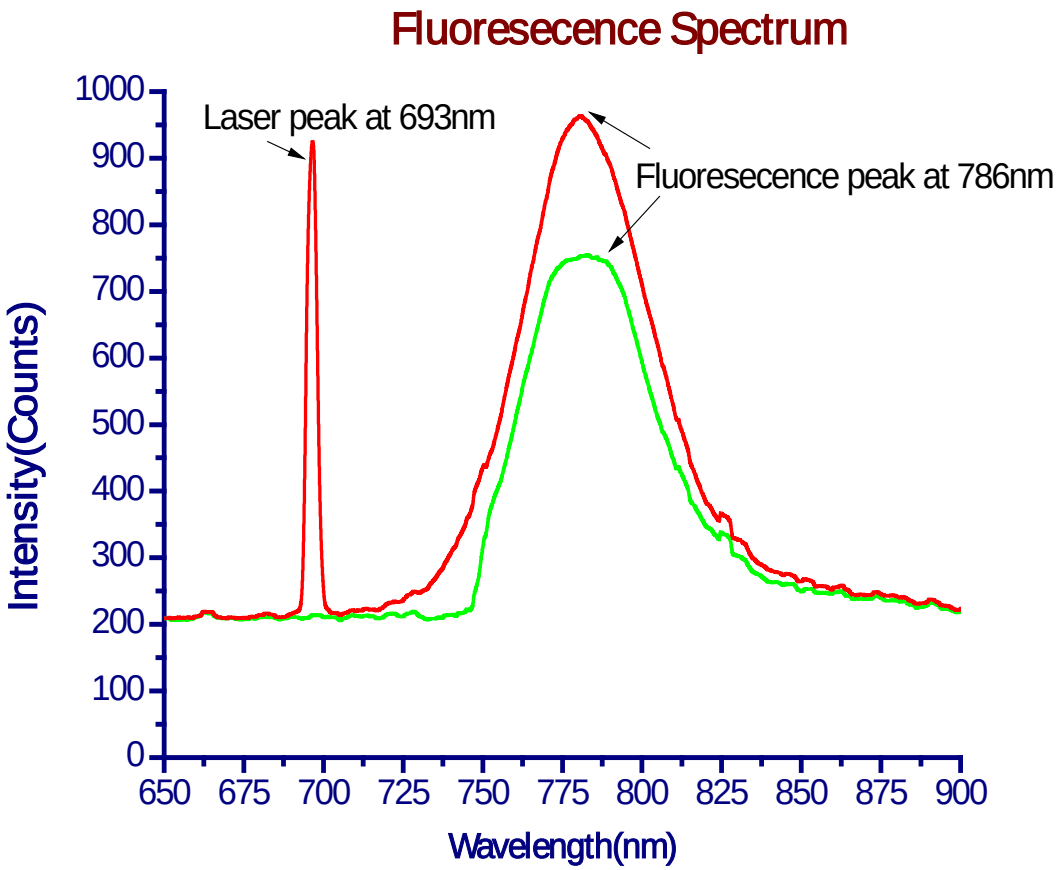

Figure 3.5: the excitation and emission spectrum of Alexa Fluor 750-βAla BBN[7-14]NH_2 studies were performed with the ocean optics spectrometer.

3.4 *In Vitro* Studies

In this study, the ability of molecular probes was conjugated to GRP receptors expressed in breast cancer and prostate cancer with minimal accumulation in normal and surrounding tissues. *In vitro* studies provide the first step for the evaluation of targeting vector conjugates to receptors on cancer

cells. The studies were performed in human prostate and breast cancer cell lines, which were cultured in Petri dishes and kept alive with a nutrition solution. Three important properties were studied using confocal microscopy: binding affinity, blocking, and internalization

3.4.1 The Studies using Confocal and Fluorescent Microscopy

In vitro binding experiments of the optical molecular probe of AF750-BetaAla-BBN[7-14]NH_2 conjugate in human breast cancer cells with T47-D cell line and prostate cancer cells with PC-3 cell line were performed to evaluate the uptake, internalization, and blocking of the conjugate. These studies were performed using an Olympus IX70 inverted microscope with an Orca ER digital camera at the Molecular Cytology Core at the Life Sciences Center at the University of Missouri.

An inverted Olympus IX70 microscope was equipped with bright field, dark field, phase contrast, differential interference contrast (DIC), and fluorescence optics. An excitation filter wheel and focus motor allowed multi-channel images in 3 dimensions. A wide range of objectives and oil objectives, 20x, 40x, 60x were used in confocal imaging. The images were acquired with a Hamamatsu Orca ER charged coupled device (CCD) camera, which is a highly sensitive, low noise device for high resolution imaging. The image acquisition and data analysis were performed with Metamorph software. Briefly, 3 x 10^6 cancer cells were suspended in RPMI 1649 media at pH 7.4 containing 2.4mg/mL HEPES, 0.1µg/mL Bacitracin, and 2 mg/mL BSA in the presence of the conjugate for a

period of 40 min at 37^0C (5% CO_2). The reaction media was centrifuged after incubation and aspirated and cells were washed with the incubation media. Then the fluorescence images were acquired by microscope. Prior to imaging the cells, they were stained by Hoechst stain (DAPI) for labeling cell nuclei. The Hoechst stains are used for labeling DNA and nuclei, used to visualize the fluorescence microscopy. The chemical structure is shown in Figure 3.6. It is excited by ultraviolet light at around 350nm and emits blue fluorescence light at an emission wavelength of 461nm. The additional ethyl group is more lipophilic and thus is more able to cross intact cell membranes. The two fluorescent probes Alexa Fluor 680 and 750 bombesin are used to study cell images for uptake, internalization, and blocking of the probe in prostate cancer cells with a cell line of PC-3 and breast cancer cells with the cell line T47-D.

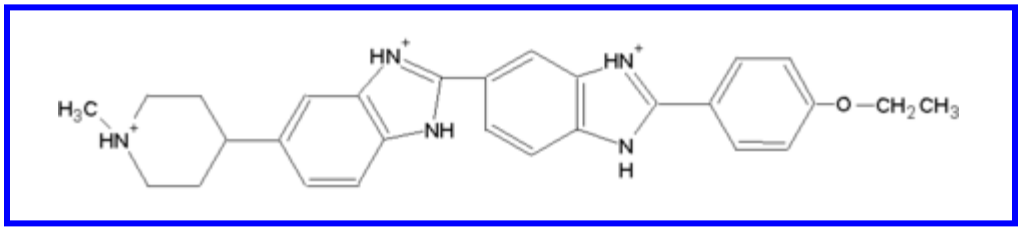

Figure 3.6: The molecular structure of Hoechst stain 33342, trihydrochloride, trihydrate with MW 615.99. (Courtesy of Molecular Probes: Invitrogen detection technologies)

3.4.2 The Binding Affinity of Optical Molecular Probe with Cancerous Cells

Initially, we performed studies to determine the efficiency of uptake, internalization, and blocking of the Alexa Fluor 680-GGG-Bombensin conjugate. The binding affinity (IC_{50}) of the Alex Fluor 680-GGG-BBN[7-14]NH_2 conjugates for the GRP receptors was evaluated using *in vitro* competitive cell-binding assays in a PC-3 human prostate cancer and T47-D breast cancer. The degree of cell-affinity in cancerous cells was determined by using Zeiss LSM 510 M-200 Axiovert confocal fluorescent microscopy at the Life Sciences Center at the University of Missouri. The images were acquired by fluorescent microscopy (figure 3.7), and the results of the microscopy studies were summarized to assess the degree of uptake, internalization, and blocking of the conjugate. The first column shows the fluorescence from the Alexa Fluor 680; the second column shows the bright light field; and third column shows the overlay image of the first and second column to examine the precise location of the fluorescence signal using Zeiss LSM Image examiner software version 3.2. The first row shows the uptake studies of the conjugate with the cells. The second row shows the internalization of cells where the conjugate on the surface of the cells was washed with ph 2.5 buffer solution in order to see the degree of affinity of the probe inside the cancer cells. The third row shows the blocking of cells where plain bombesin was introduced in cells prior to the conjugate.

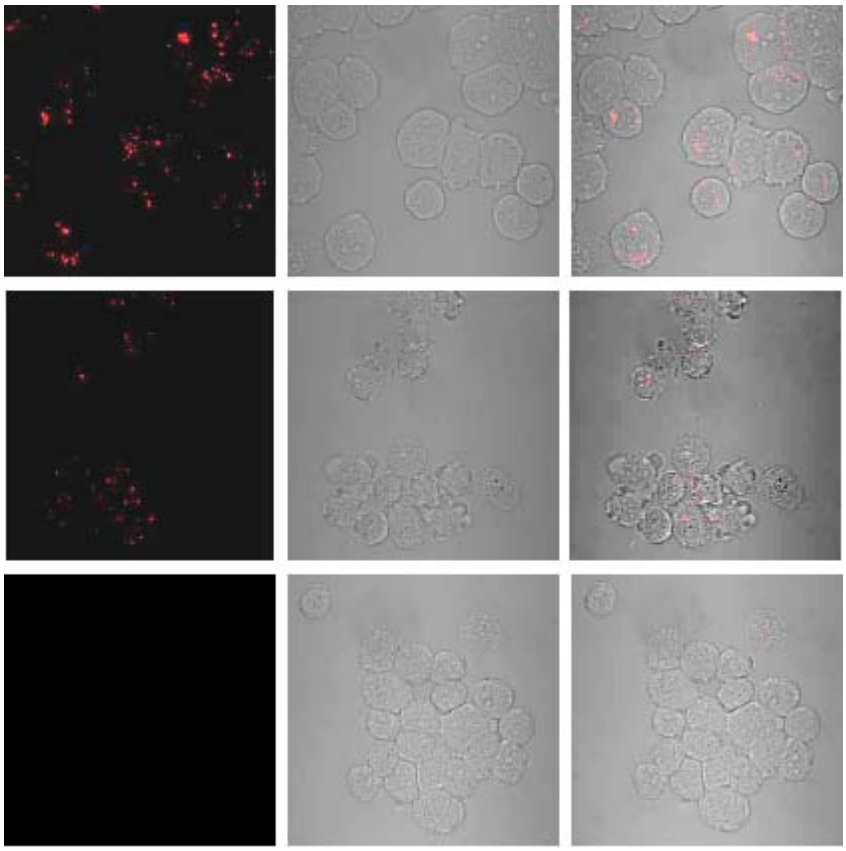

Figure 3.7: The fluorescent confocal microscopy images Alexa Fluor 680-BBN[7-14] NH_2 conjugate in PC-3 prostate cancer cells**. The first row:** uptake**, second row:** internalization, **third row:** blocking studies. **The first column:** fluorescent images**, second column:** bright light field**, and third column:** overlay image

For the Alexa Fluor 750 bombesin peptide, the images were acquired in two steps: the incubated cells were stained by Hoechst stain (DAPI) for 20 minutes, then fluorescent images were acquired. The objective used for collecting images was 40x magnification of the U Apo/340 objective with numerical aperture of 1.35; the immersion medium was oil. The field of view was 216.8 x 165.2 (µm). Initially, the cell images ware acquired with a DAPI filter to

under illuminate the blue light to see the labeled nuclei, as shown in the figure 3.8 with a blue color in the second column. The parameters used were gain 150, exposure time 125msec, binning 1, and live bin 2. The fluorescence images were acquired using a He-Ne laser and long-pass filter cy7 (750nm), as shown in he figure 3.8 with red color from the AF-750 molecule. Upon image acquisition, the two images were overlaid to examine the precise location of the fluorescence signal for uptake, internalization, and blocking of the probe AF750-BetaAla-BBN[7-14]NH_2 Conjugate in human prostate and breast cancer cells. The degree of molecular optical probe trapped in the cells was determined by removal of surface-bound molecules, using a pH 2.5 (0.2M acetic acid and 0.5M NaCl) buffer wash and following the wash with incubation media, as shown below, The internalized cell-associated molecular optical probe AF750-BetaAla-BBN[7-14]NH_2 Conjugate was also determined as shown in figure 3.8.

In order to assess the degree of receptor specificity of these conjugates in human breast T-47D and prostate PC3 cancerous cells, a blocking study was performed. The 5µg of native Bombesin (1-14) peptide was incubated with cells prior to incubation with Alexa Fluor 750-BetaAla-Bombesin [7-14] NH_2 Conjugate as shown in Figures 3.7, 3.8 and 3.9. Results of these studies clearly demonstrate the effectiveness of the molecular optical probe with high affinity and selectivity to specifically target the GRP receptor over-expressed on T-47D breast cancer cells and PC3 prostate cancer cells.

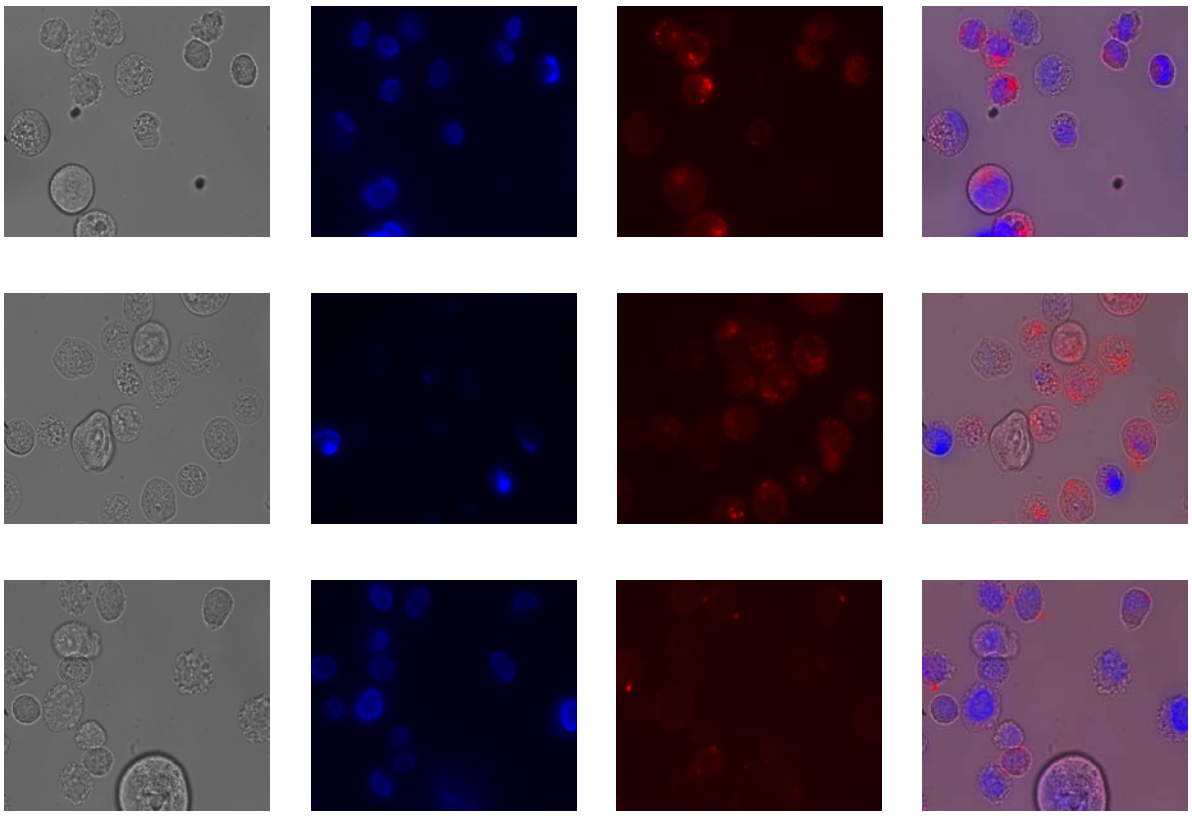

Figure 3.8 The fluorescent confocal microscopy images of Alexa Fluor 750-BBN[7-14]NH_2 conjugate in T47-D breast cancer cells**. The first row:** uptake**, second row:** internalization, **and third row:** blocking studies. **The first column:** bright field images**, second column:** Hoechst (DAPI) strain image**, third column:** fluorescence image of cells, and **fourth column:** overlay images of bright field, DAPI dye, and fluorescence.

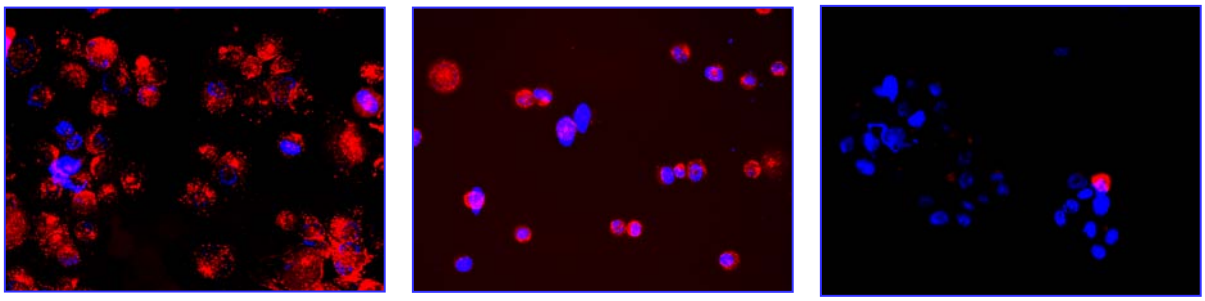

Figure 3.9: Confocal microscopic image of conjugate for uptake, internalization, and blocking studies of PC-3 prostate cancer cells, *in vitro* cell binding affinity of Alexa Fluor 750-βAla-BBN [7-14] NH_2 conjugate.

3.5 *In Vivo* Studies

In vivo studies showed the effect of the optical molecular probe in a mouse model. Since human cancer cells can be implanted in mice, the uptake and blocking experiments can be performed in the mouse model to examine the human cancer cell binding reaction to the BBN conjugate. In addition, an evaluation of these conjugates for fluorescence imaging can be performed by using optical fluorescence in a small animal imaging system.

3.5.1 Introduction

The development of fluorescence molecular based drugs has been progressing at a rapid pace, necessitating the development of diagnostic methods for identification of molecular targets for individual tailoring of therapy. Currently, the clinical standard of molecular imaging is nuclear imaging, whether for planar scintigraphy imaging with gamma emitters or for tomographic imaging with gamma or positron emitters [12]. The use of near-infrared excitable

fluorescent molecules conjugated to targeting moieties can also be used to provide a new, non-ionizing form of molecular imaging. Conjugation of a fluorophore to the GRPr can give high fluorescent contrast for tumor cells compared with the normal cells [7,13]. For instance, Achilefu et al [14] and Becker et al [15] have developed a highly somatostatin (sst2) receptor-specific tricarbocyanine based peptide-dye conjugate to image the tumor that tends to over-express the sst2 receptor. Zheng et al [16] have targeted another kind of receptor-LDLr, which also tends to over-express on several types of tumor cells. Another interesting type of molecular fluorescent marker has been developed by Weissleder et al [17]. They used the protease-activated probes containing auto-quenched fluorescent molecules through fluorescence resonance energy transfer (FRET) that can be cleaved by tumor-specific proteases and then fluoresce. Through this kind of approach, high fluorescent contrast is demonstrated in a tumor [17, 18,19].

Combining the molecular probes and optical imaging techniques will yield the high sensitivity and specificity for cancer detection. This work has significance for early detection of cancerous tissue cells at the molecular level, before the anatomic changes become apparent [20]. Therapy can be applied in the early stages of neoplasia to achieve high survival rates. While numerous challenges associated with the administration of a new contrast agent must be overcome before fluorescence enhanced optical imaging can be implemented in the clinic, the ability to track molecularly targeted dyes in small animals demonstrates that tomographic imaging can be accomplished using both planar

and point illumination/collection geometries [21]. Optical imaging apparently has the same capabilities as nuclear scintigraphy and tomographic imaging with PET and SPECT [22, 23].

3.5.2 Optical Imaging System for Uptake and Blocking Studies in Mice

The study of the uptake and blocking of the optical molecular probe in mice was performed using the IVIS Xenogen system. The IVIS Imaging System 200 series is an integrated imaging system consisting of a CCD camera mounted on a light-tight specimen chamber, a camera controller, a cryogenic cooler, a fluorescence light source, and a Windows-based computer system for data acquisition and analysis. The apparatus used for cooling or controlling the camera and other chamber functions is enclosed within a sound limiting enclosure beneath the specimen chamber. All components except the computer are integrated into a single, moveable chassis, as shown in Figures 3.10, 3.11, 3.12 and 3.13.

The Xenogen IVIS imaging system 200 series is a highly sensitivity, low noise, in vivo imaging technology platform that allows non-invasive visualization and tracking of cellular and genetic activity within a living organism in real time. Specific genes, cells or organisms are “tagged” with a fluorophore. When the tagged entity is active, it glows. The emitted light corresponds to the number and location of the tagged entities. With this information, we can observe the spread of disease, or the effects of a drug throughout the system, non-invasively. The IVIS Imaging System 200 series is capable of taking these very low light level

images, storing them, and displaying them for subsequent analysis. The sensitive range of the CCD camera sets the wavelength range for fluorescence applications from 400nm to 950nm. The internal components of Xenogen system and the alignment of the projection of laser light for illumination of mice and its position to acquire an image by the CCD camera are shown in Figure 3.10 and 3.11

Figure 3.10: The Xenogen IVIS 200 system. (Courtesy of the Xenogen Corp, Alameda, CA)

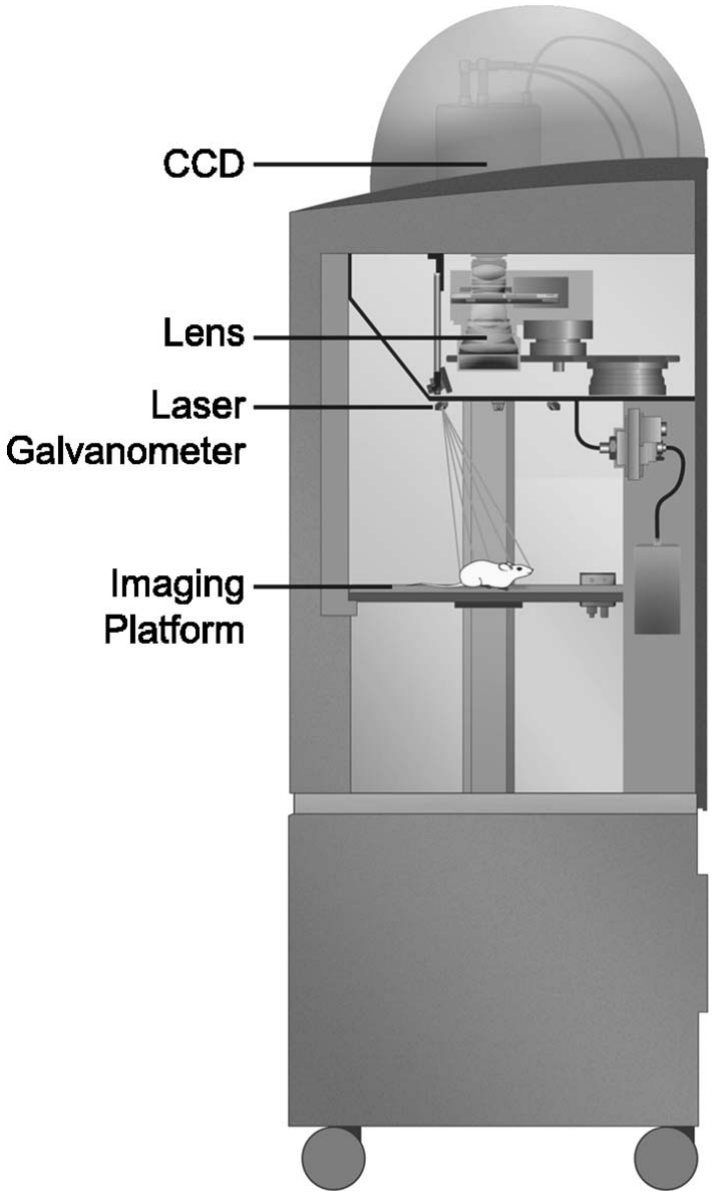

Figure 3.11: The Xenogen IVIS 200 system with its internal components.

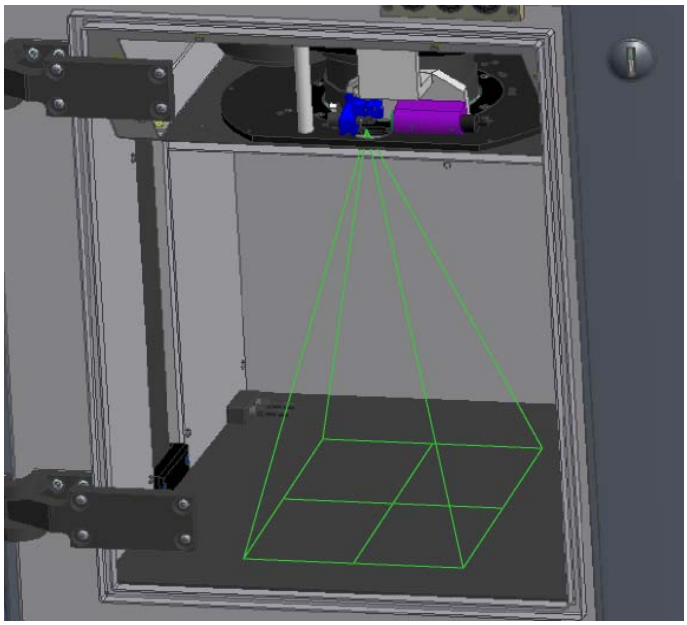

Figure 3.12: Alignment light projector

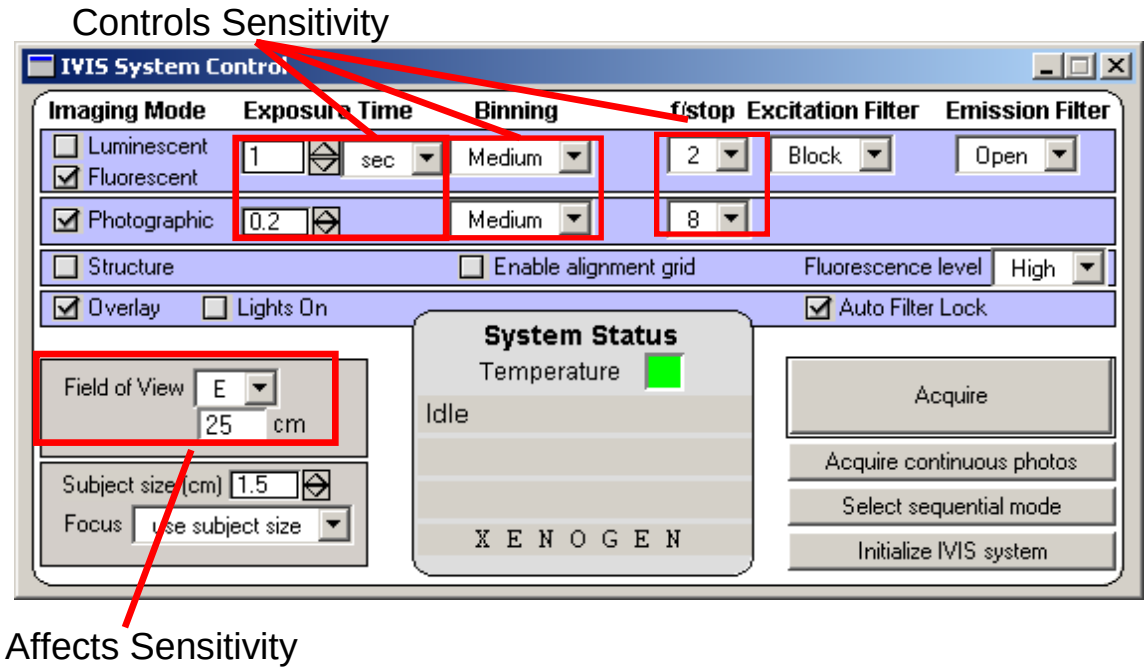

Figure 3.13: Data acquisition window on Xenogen IVIS 200 Imaging System using Living Image Software version 2.5.

3.5.3 *In Vivo* Fluorescent Signal Enhancement of the Tumors

The uptake and blocking studies of the optical molecular probe were performed using severely compromised immunodeficient (SCID) mice bearing human PC-3 prostate tumor and human T-47D breast tumor xenografts. All animal studies were conducted in accordance with the highest standards of care as outlined in the NIH guide for Care and Use of Laboratory Animals and the Policy and Procedures for Animal Research at the Harry S. Truman Memorial Veterans Hospital. Four to five week old SCID mice were obtained from Taconic (Germantown, NY). SCID mice were inoculated with 10×10^6 PC-3 cells bilateral flank. The tumor sized ranged from 1 to 1.2cm in diameter. All studies were performed on the Xenogen IVIS 200 system, which is housed at the Biomolecular Imaging Center at the VA Hospital. Data acquisition was performed using Living Image Software, version 2.5. In vivo investigations in SCID mice bearing xenografted PC-3 prostate cancer cells and T-47D breast cancer lesions demonstrated the ability of the optical molecular probe Alexa Fluor 750 to specifically target tumor tissue with high selectivity and specificity.

The fluorescent signal enhancements were assessed in SCID mice with solid tumor xenografts. Intravenous administration of the conjugate significantly enhanced the tumor image contrast, as shown in figures 3.14, 3.15, 3.16 and 3.17. The enhancement was observed as early as 10 minutes after administration and increased gradually; reaching the maximum at 30 minutes to 3 hours. After that a gradual decrease in the signal enhancement was observed. The enhancement pattern became relatively consistent from 1 to 3 hours. Some

areas of the tumors were strongly enhanced initially, while other areas were weakly enhanced. The signals from the strongly enhanced region decreased much more slowly than the signals from the region with weak enhancement. For small tumors, the enhancement was relatively uniform and the enhancement was usually observed starting from the peripheral area of tumor. The maximum enhancement was usually observed at 30 to 60 minutes after injection. The image contrast enhancement started from the peripheral area to the center of the tumors and was relatively uniform within tumors, irrespective of the sizes studied. The signal enhancement decreased rapidly and returned to baseline within 3 hours.

To understand whether the probe was preferentially accumulated in tumors and whether the fluorescent signal was optically detectable in vivo, tumors were imaged using the Xenogen IVIS 200 series optical imaging. The fluorescent signal was clearly detectable as early as 10 minutes and reached the maximum intensity at about 30 minutes to 3 hours after intravenous injection of the Alexa Fluor 750- βAla-BBN [7-14] NH_2 Conjugate, as shown in figures 3.14, 3.15. Following intravenous injection, the probe was rapidly distributed throughout the body. However, the probe was rapidly washed out from organs but not from solid tumors. The uptake of the probe in tumors was enhanced because of binding to GRPr in the tumor.

Initially, the animals were anesthetized, using 2.5% isoflurane. Prior to anesthesia, the Alexa Fluor 750-βAla-BBN[7-14]NH_2 Conjugate was injected through the tail vien. For assessment of the normal uptake of the conjugate,

50µL of phosphate buffered saline was injected via the tail vein into a SCID mouse bearing PC-3 human prostate cancer tumors on the left and right flanks, followed by administration of 50µg of Alexa Fluor 750- βAla-BBN [7-14] NH_2 in 100µL of isotonic saline. The *in vivo* blocking experiment was performed with 50µg of commercially available BBN(1-14) injected into the tail vein of a SCID mouse bearing PC-3 xenografted tumors 10 minutes prior to injection of the Alexa Fluor 750- βAla-BBN [7-14] NH_2 conjugate. All mice were immediately imaged using a Xenogen IVIS 200 series system (Xenogen Corp., Alameda, CA). Prior to the intravenous injection, a baseline image was collected. The mice were placed in the temperature-controlled imaging chamber under zero-light conditions. All images were acquired with exposure time 0.05 sec, emission and excitation filter cy5.5, binning medium, a low fluorescence lamp level, field of view 12.7cm and f/stop 2, 8. All the images were analyzed using Living Image Software. Figures 3.15, 3.16, and 3.17, clearly show that the uptake and blocking assessment started after the intravenous administration of the molecular probe in the SCID mice, at 10 minutes and to 1 hour. Mice were euthanized by CO_2 after 1 hour studies of normal uptake and blocking studies. Prior to euthanasia, MRI imaging was performed to correlate anatomical information with optical images of tumors as shown in figures 3.18, and 3.19.

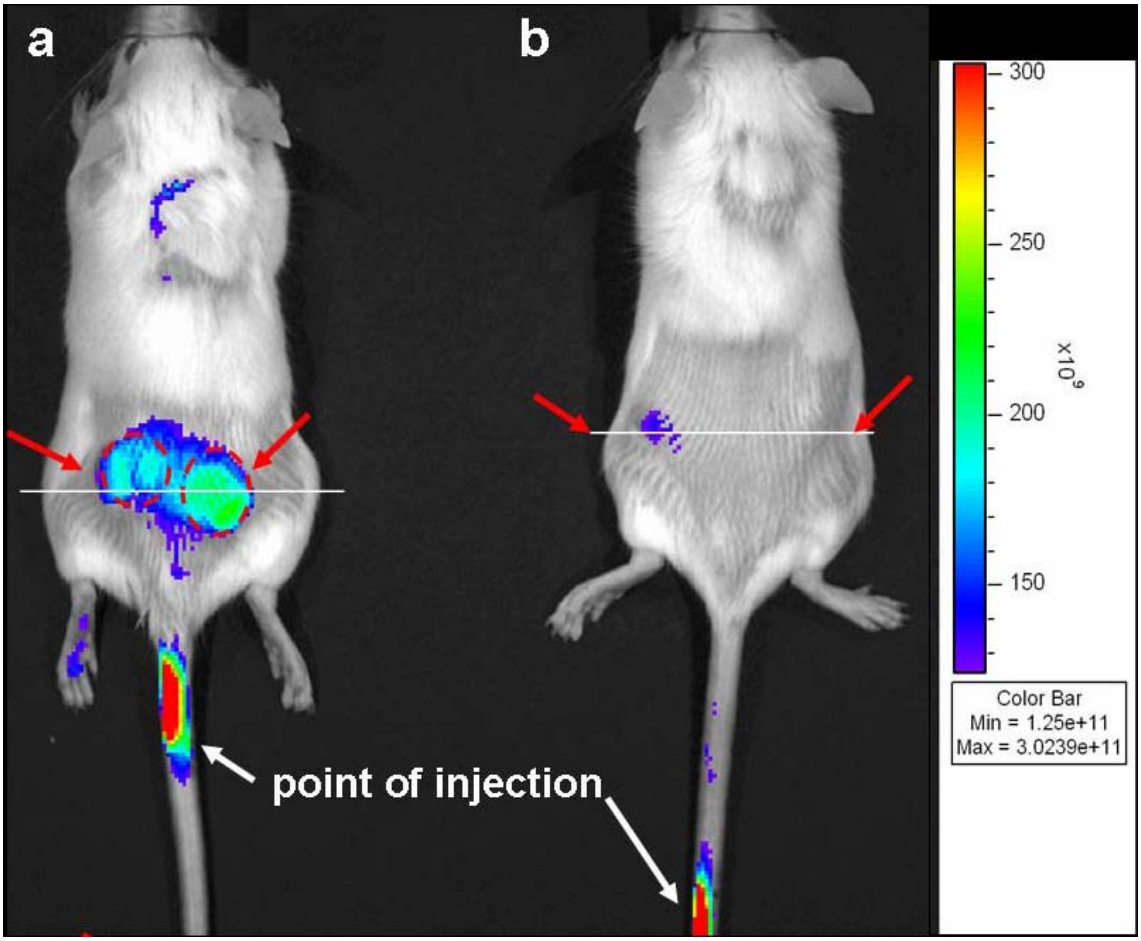

Figure 3.14: *In vivo* Uptake and Blocking Experiment of Molecular Optical Probe AF 680 conjugate in SCID Mice Bearing Human T-47D Breast Cancer Cell Xenografts. (From Ref.7)

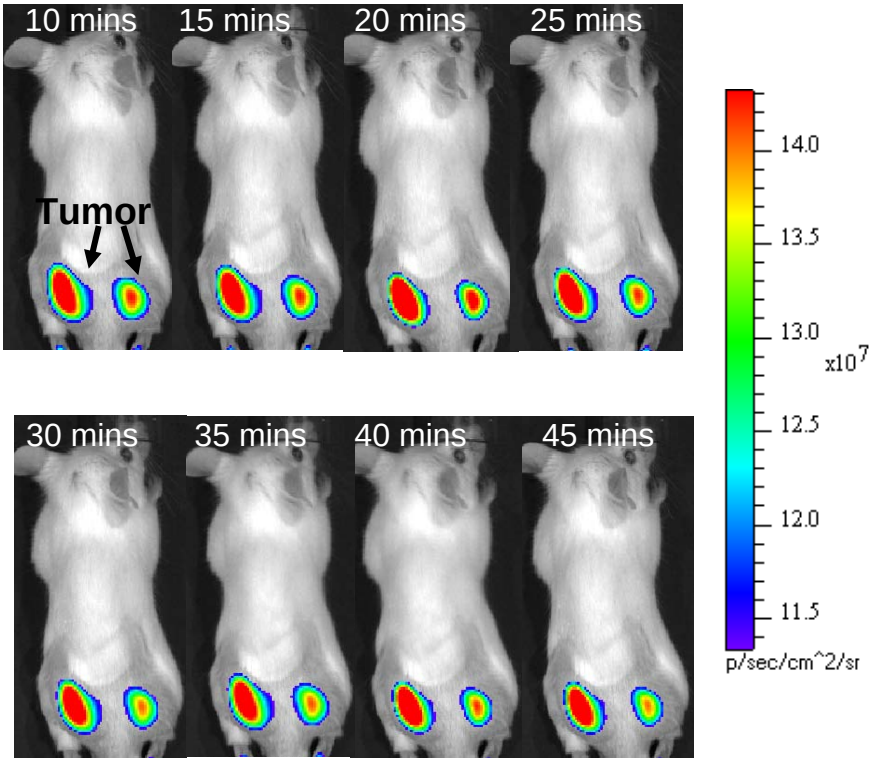

Figure 3.15: The normal uptake of dynamic change of the fluorescent signal in tumors. The arrow shows the location of tumor with parameters: Binning is medium, Exposure time is 0.05 sec, FOV is 12.7cm, Subject height is 1.5cm, lamp level is low, Filter is cy5.5 and f/stop is 2,8.

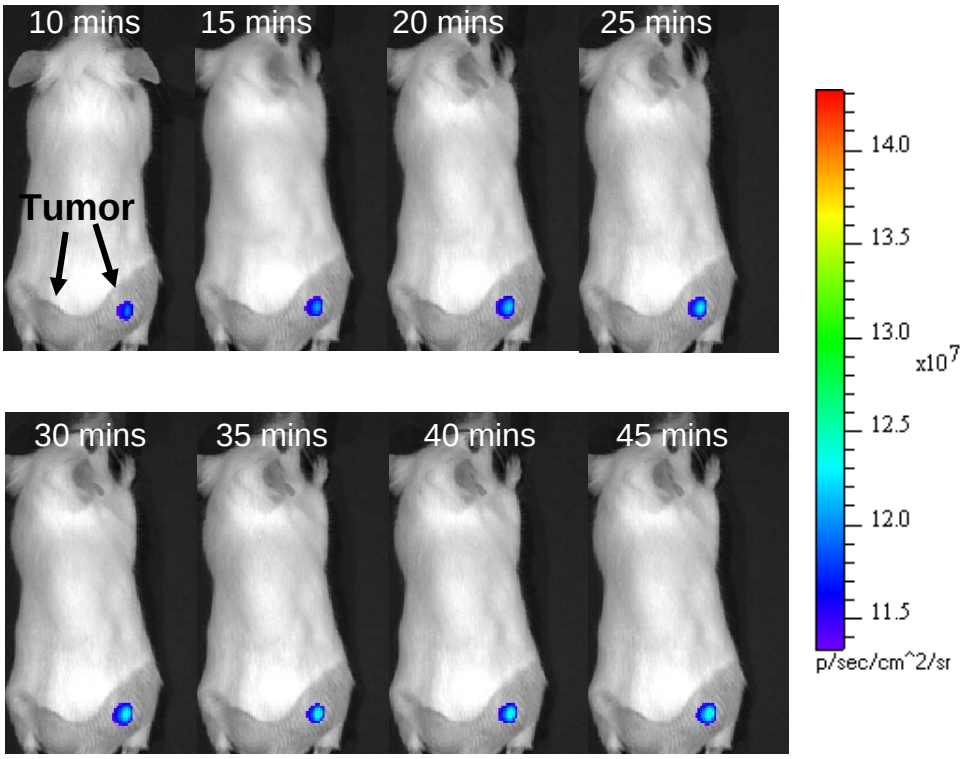

Figure 3.16: The normal blocking assessment of dynamic change of the fluorescent signal in tumors. The arrow shows the location of tumor with parameters: Binning is medium, Exposure time is 0.05 sec, FOV is 12.7cm, Subject height is 1.5cm, lamp level is low, Filter is cy5.5 and f/stop is 2,8.

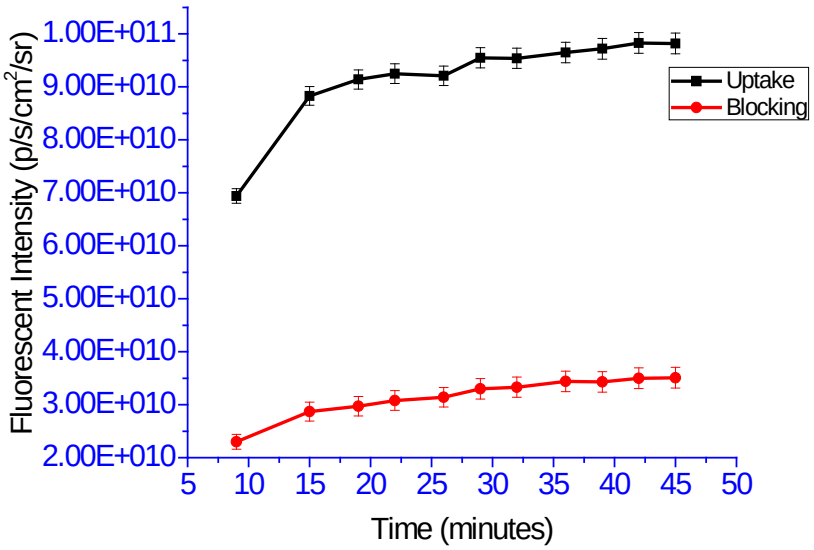

Figure 3.17: The dynamic change of fluorescent intensity signal from tumors of SICD mice over time.

3.6 MRI Studies of Tumors in SCID Mice

For the MRI study, the animal was anesthetized using 2% isoflurane and positioned with the tumor at the center of the coil. The physiologic condition of the animals was monitored using a respiratory gating device during the scanning. The tumor was scanned in the perpendicular direction of the tumor and animal skin interface. Diffusion weighted spin echo multi-slice images were used for imaging studies, with repetition time (TR) 2000 milliseconds and echo time (TE) 37 milliseconds. Slice thickness was 1mm with no gap, diffusion gradients in x, y,

z directions, 7-11 slices, image matrix size 256 x 256, field of view (FOV) 30mm x 30mm, number of averages 2 and the b factor 1700 s/mm^2. All MRI images were acquired on a 7Tesla Micro MRI imaging system with 210mm diameter in bore Varian Unity Inova MRI system equipped with a quadrature driven birdcage coil of 38mm internal diameter (Varian Inc, Palo Alto, CA).

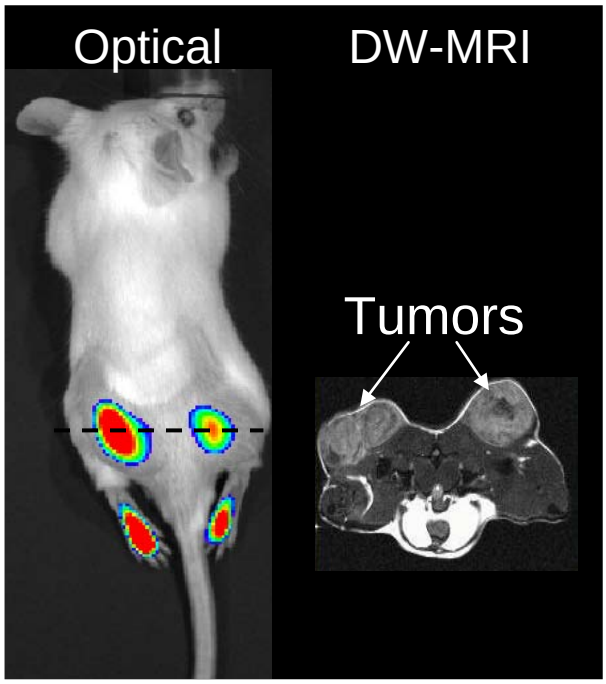

Figure 3.18: The optical and MR imaging of diffusion weighted images of normal uptake tumor with parameters: TR is 2000 msec, TE is 37 msec, FOV is 30mm x 30mm, b factor is 1700 s/mm^2, averages is 2, matrix size is 256 x 256 and the arrow shows the location of tumors. (Courtesy to Dr. Lixin Ma)

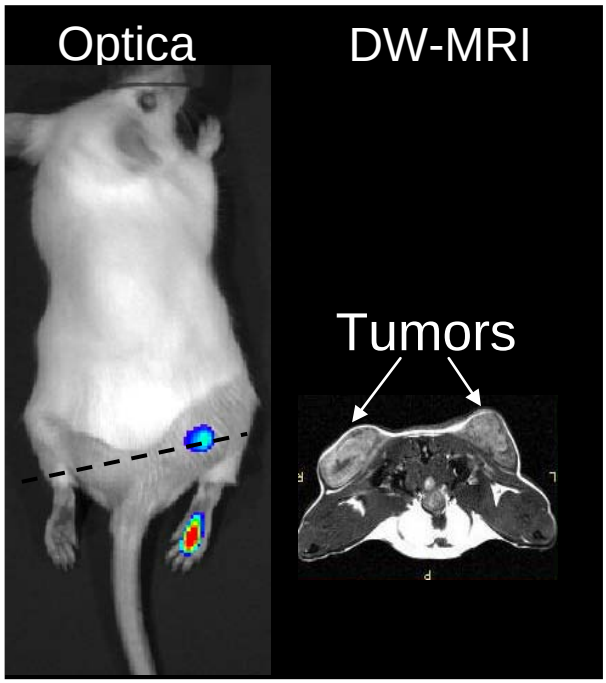

Figure 3.19: The optical and MR imaging of diffusion weighted images of normal blocking tumor with parameters: TR is 2000 msec, TE is 37 msec, FOV=30mm x 30mm, b factor is 1700 s/mm^2, averages is 2, matrix size =256 x 256. The arrow shows the location of tumors. (Courtesy to Dr. Ma)

3.7 Ex-Vivo Studies

The ex-vivo studies were performed in order to see the binding affinity of the conjugate to tumors for uptake and blocking in the mice. As the optical imaging indicates, the binding affinity of molecular optical probe AF750-βla-BBN [7-14]NH_2 Conjugate in the SCID mice for normal uptake studies and blocking

studies were performed to assay the binding affinity of conjugate in tumors in prostate and breast cancer. The animals were sacrificed in a CO_2 chamber. After sacrificing the animals, optical imaging was performed to monitor whether the fluorescent signal from the tumors was detectable for both the mice used for uptake and blocking studies of the molecular probe.

After acquiring the post-MRI images of the uptake and blocking images of mice, the mice were euthanized in the CO_2 chamber. The mice were dissected for organs and tissues were weighed. The organs are placed in a tray on the black background in the following order: L-tumor, R-tumor, Kidneys, Pancreas, Muscle, L-Mammary, R-Mammary, Liver (w/o gall bladder), Stomach, Small Intestine, and Large Intestine, as shown in figures 3.20 and 3.21. Optical imaging was performed using the Xenogen IVIS system for Biodistribution of Alexa Fluor 750- BetaAla-BBN [7-14] NH_2 Conjugate in the tumors and organs of mice, as shown in the figures 3.22 and 3.23. The fluorescent signal data were analyzed using Living Image Software version 2.5 (Xenogen Corp., Alameda, CA). In figure 3.20, we can see the fluorescent intensity signal expressed in photos/cm2/sec/sr for uptake of the Alexa Fluor 750- βAla-BBN [7-14] NH_2 Conjugate in the left and right tumors is greater than in other organs. This clearly, indicates that the Alexa Fluor 750- βAla-BBN [7-14] NH_2 Conjugate has more binding affinity for the GRP receptor, which, in turn, suggests that binding affinity is greater for cancerous cells than normal cells. From the figure 3.21, we can see the blocking of the conjugate in left and right flank is relatively small when compared with the uptake of tumors.

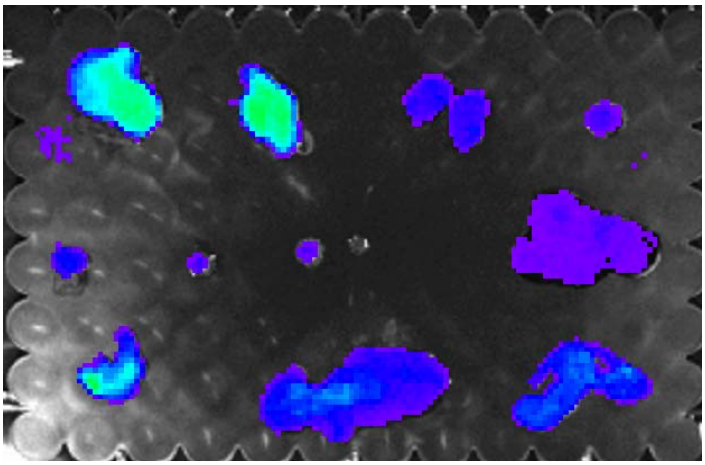

Figure 3.20: The ex-vivo studies of normal uptake of molecular probe (AF 750-βAla-BBN [7-14] NH_2 Conjugate). The arrangement of organs and tumors on black background plate are: R-tumor, R-tumor, Kidneys, and Pancreas, (Top row): Muscle, L-Mammary, R-Mammary, and Liver, (w/o gall bladder) (Middle row): Stomach, Small Intestine, and Large Intestine (Bottom row).

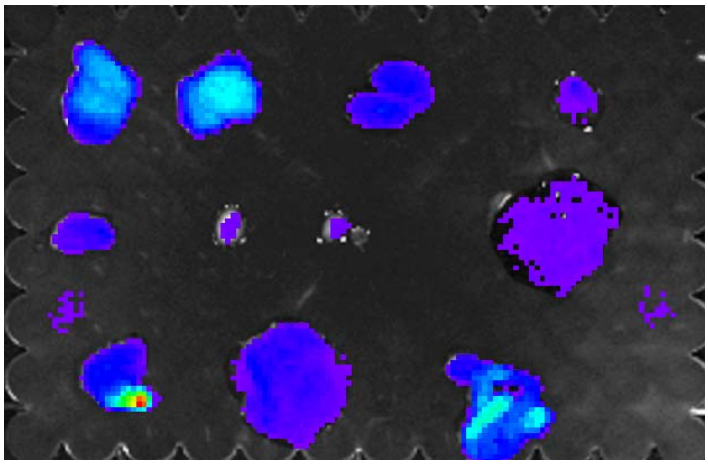

Figure 3.21: The ex-vivo studies of blocking of molecular probe (AF 750-βAla-BBN[7-14] NH_2 Conjugate). The arrangement of organs and tumors on black background plate are: R-tumor, R-tumor, Kidneys, and Pancreas, (Top row): Muscle, L-Mammary, R-Mammary, and Liver, (w/o gall bladder) (Middle row): Stomach, Small Intestine, and Large Intestine (Bottom row).

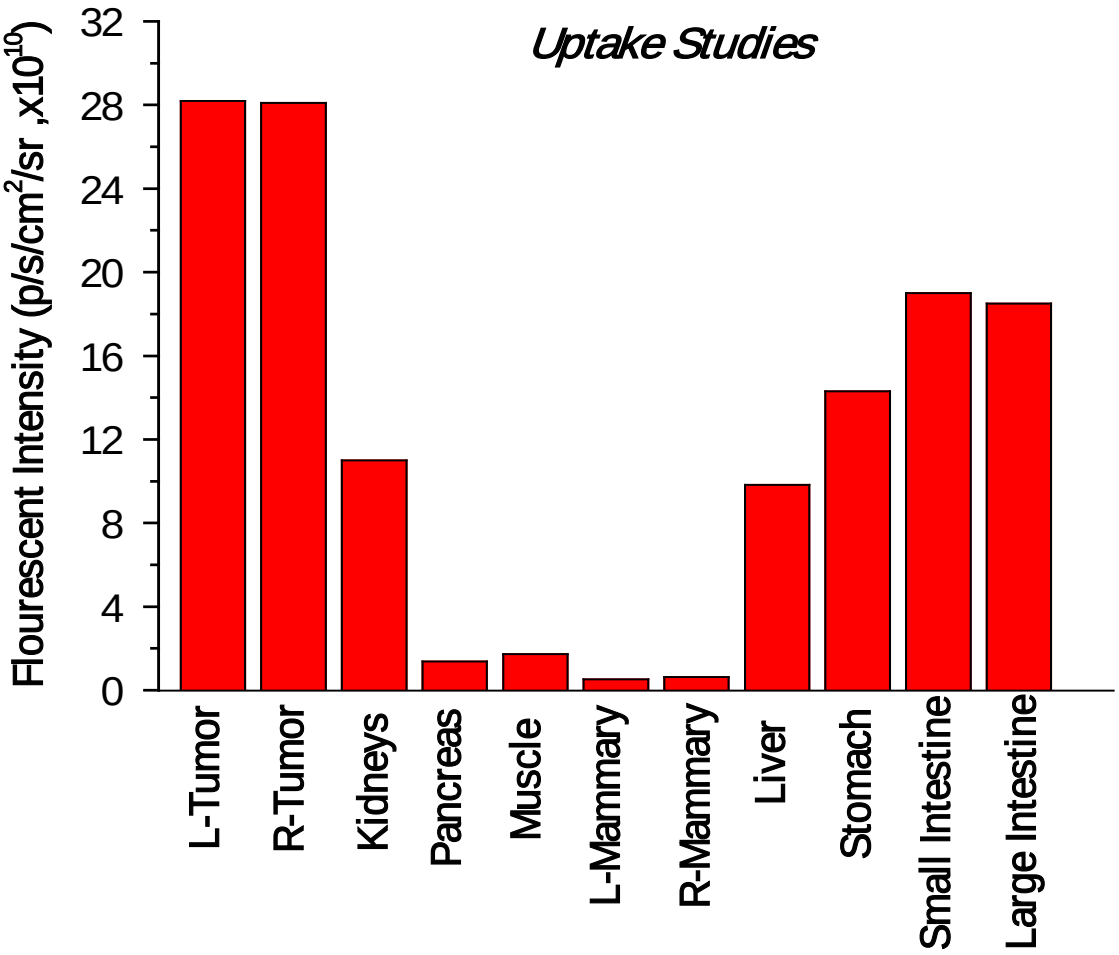

Figure 3.22: The Biodistribution of molecular probe (AF750- βAla-BBN [7-14] NH_2 Conjugate) in tumors and tissues. Organs versus fluorescent signal for uptake studies indicating the binding affinity of probe in tumors is more when compared with other tissues of body.

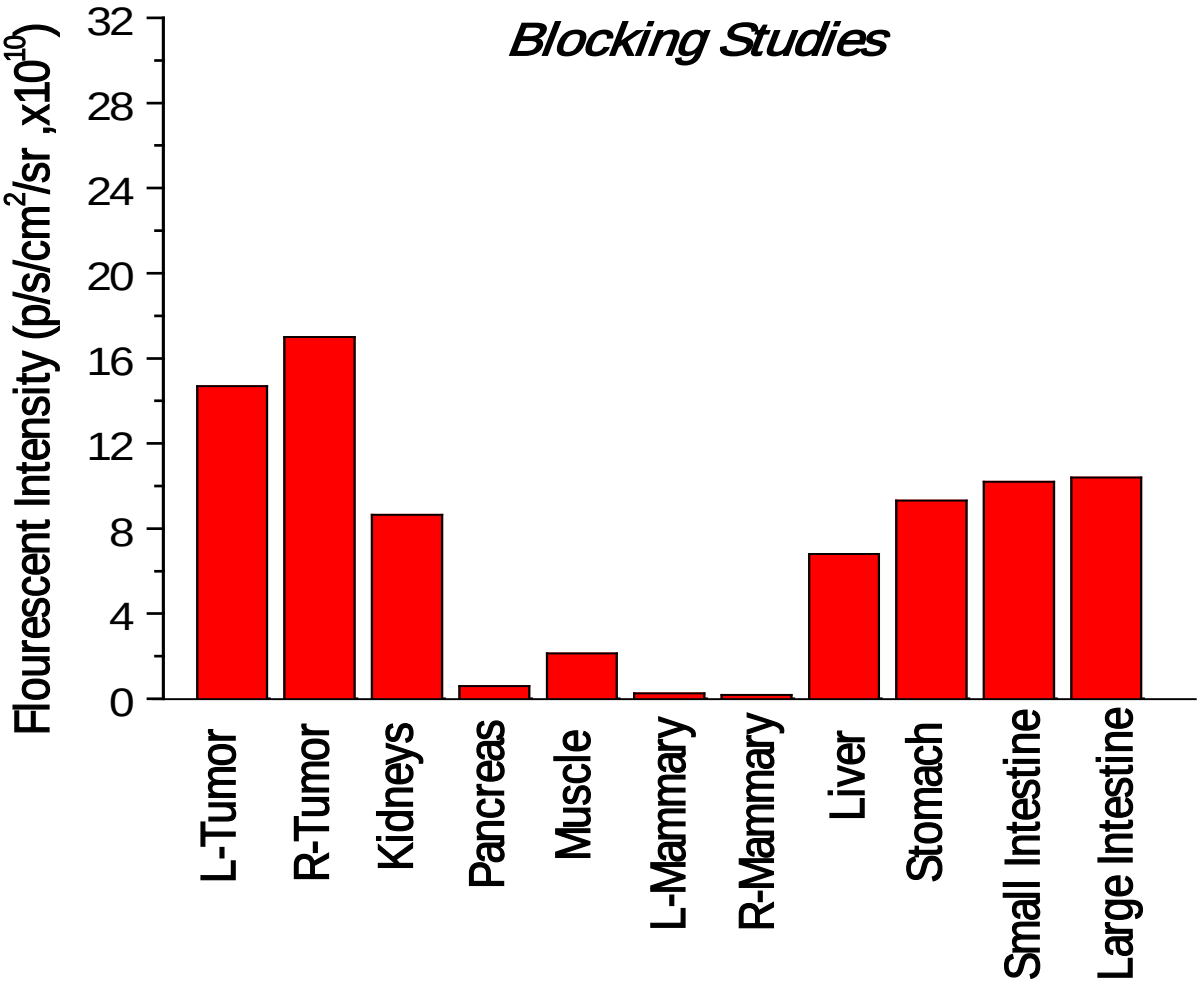

Figure 3.23: The Biodistribution of molecular probe (AF 750- βAla-BBN [7-14] NH_2) in tumors and tissues. Organs versus fluorescent signal for blocking studies indicating the fluorescent signal of probe in tumors is less when compared with uptake studies of tumors and tissues.

Bibliography:

1. Ntziachristos V, Yodh AG, Schnall M and Chance B. “Concurrent MRI and diffuse optical tomography of breast after indocyanine green enhancement”. Proc. Natl. Acad. Sci, Vol. 97, 2767-2772 (2000)
2. Rhine WD, Benaron A, Darceuil HE, deCrespigny A, Cheong WF. “Simultaneous time of flight adjusted near infrared spectroscopy and magnetic resonance imaging of immature rabbit hypoxic-ischemic encephalopathy”. Pediatr. Res, Vol. 39 (1996)
3. Wagnieres GA, Star WM and Wilson BC. ”*In vivo* fluorescence spectroscopy and imaging for oncological applications”. Photochem. Photobiol, Vol. 68, 603-632 (1998)
4. Pogue, BW, Geimer S, McBride TO, Jiang SD, Osterberg UL. “Three-dimensional simulation of near-infrared diffusion in tissue: Boundary condition and geometry analysis for finite element image reconstruction”. Appl. Optics, Vol. 40, 588-600 (2001)
5. Hawrysz DJ and Sevick-Muraca EM. “Development towards diagnostic breast cancer imaging using near-infrared optical measurements and fluorescent contrast agents”. Neoplasia, Vol. 2, 388-417 (2000)
6. Hebden JC, Veenstra H, Dehghani H, Hillman EMC, Schweiger M. “Three-dimensional time-resolved optical tomography of a conical breast phantom”. Appl. Optics, Vol. 40, 3278-3287 (2001)
7. Ma L, Yu P, Veerendra B, Rold TL, Retzloff L, Prasanphanich A, Sieckman G, Hoffman TJ, Volkert WA, and Smith CJ. “In Vitro and in vivo

evaluation of alexa fluor 680-BBN[7-14]NH2 peptide conjugate: A high-affinity fluorescent probe having high selectivity for the GRP receptor". Molecular Imaging, Vol. 6(3), 171-180 (2007)

8. Ma L, Brown A, Kujala NK, Zhai H, Smith J, Figureoa S, Yu P, Hoffman T, and Volkert W. "Functional apparent diffusion coefficient mapping the uptake of tumor-targeting bombesin probes in human breast and prostate cancer xenografts". Proc Intl Soc Mag Reson Med, Vol. 16, 2813 (2008)
9. Balasubramanian S, Carmignani B, Kujala NK, Pacheco D, Ma L, Smith J, Hoffman T, Volkert W, and Yu P. "Using fluorescence molecular tomography for multimodality fusion imaging". Proc. SPIE, Vol. 6431, 643110 (2007)
10. Adams KE, Ke S, Kwon S, Liang F, Fan Z, Lu Y, Hirshi K, Mawad ME, Barry MA and Sevick-Muraca EM. "Comparison of visible and near-infrared wavelength-excitable fluorescent dyes for molecular imaging of cancer". J. Biomed. Optics, Vol. 12, 024017-22 (2007)
11. Lakowicz JR, "Principles of fluorescence spectroscopy". Plenum Press, New York (1983)
12. Smith CJ, Sieckman GL, Owen NK, Hayes DL, Mazuru DG, Volkert WA, Hoffman TJ. "Radiochemical investigations of [^{188}Re($H_2O(CO)_3$-diaminopropionic acid-SSS-bombesin(7-14)NH_2]: Syntheses, radiolabeling and in vitro/in vivo GRP receptor targeting studies". Anticancer Res, Vol. 23, 63-70 (2003)

13. Achilefu S, Jimenez HN, Dorshow RB, Bugaj JE, Webb EG. “Synthesis, In vitro receptor binding, and *in vivo* evaluation of fluorescein and carbocyanine peptide-based optical contrast agents”. J. Med. Chem, Vol. 45, 2003-2015 (2002)
14. Achilefu S, Dorshow RB, Bugaj JE and Rajagopalan R. “Novel receptor-targeted fluorescent contrast agents for in vivo tumor imaging”. Invest. Radiol, Vol. 35, 479-485 (2000)
15. Becker A, Hessenius C, Licha K, Ebert B, sukowski U, Semmler W, Wiedenmann B and Grotzinger C. “Receptor-targeted optical imaging of tumors with near-infrared fluorescent ligands”. Nat. Biotechnol, Vol. 19, 327-331 (2001)
16. Zheng G, Li H, Yang K, Blessington D, Licha K, Lund-Katz S, chance B, and Glickson JD. “Tricarbocyanine cholesteryl laurates labeled LDL: New near infrared fluorescent probes (NIRFS) for monitoring tumors and gene therapy of Familial hypercholesterolemia”. Bioorg. Med. Chem. Lett, Vol. 12, 1485-1488 (2002)
17. Weissleder R, Tung CH, Mahmood U and Bogdanov A. “In vivo imaging of tumors with protease-activated near-infrared fluorescent probes”. Nat. Biotechnol, Vol. 17, 375-378 (1999)
18. Eppstein MJ, Hawrysz DJ, Godavarty A, and Sevick-Muraca EM. “Fluorescence-enhanced optical imaging in large tissue volumes using gain modulated ICCD camera”. Phys Med Biol, Vol. 48, 1701-1720 (2003)

19. Ntziachristos V, Weissleder R. “Charge-coupled-device based scanner for tomography of fluorescent near-infrared probes in turbid media”. Med Phys, Vol. 29(5), 803-809 (2002)
20. Eva M. Sevick-Muraca. “Fluorescence-enhanced optical imaging and tomography for cancer diagnostics”. IEEE, 1482-85 (2004)
21. Godavarty A, Eppstein MJ, Zhang C, Theru S, Thompson AB, Gurfinkel, Sevick-Muraca EM. “Fluorescence-enhanced optical imaging in large tissue volumes using a gain modulated ICCD camera”. Phys Med Biol, Vol. 48(21), 1701-1720 (2003)
22. Graves EE, Ripoll J, Weissleder R, Ntziachristos V. “A submillimeter resolution fluorescence molecular imaging system for small animal imaging”. Med Phys, Vol. 30, 901-911 (2003)
23. Prasanphanich A, Nanda PK, Rold TL, Ma L, Lewis, MR, Hoffman TJ, Sieckman GL, Figueroa SD, and Smith CJ. “[^{64}Cu-NOTA-8-Aoc-BBN(7-14)NH_2] conjugate: A novel targeting vector for positron emission tomographic imaging of gastrin releasing peptide receptor-expressing tissues” PNAS, Vol.104, 12462-7 (2007)

Chapter 4

Phantom Studies and Design

4.1 Introduction

In this chapter an overview of various types of tissue simulating phantoms and their applications are outlined. For mimicking the properties of human or animal tissues, tissue-simulating objects are developed that are considered tissue-simulating phantoms. For most of the diagnostic imaging systems and therapeutic systems, phantoms are required to initially test the newly designed system, to minimize the noise, and to check the performance of the system for quality control.

In the early 1980s, the development of tissue-simulating phantoms for near-infrared imaging of tissues was first attempted [1]. Early studies of tissue phantoms were focused on creating regular-shaped phantoms that mimicked the reduced scattering coefficient and absorption coefficient in tissues at specific wavelengths. In recent years, the focus has shifted to developing phantoms with optical properties over a broader wavelength range, matching the full spectrum of reduced scattering coefficients and absorption coefficients. The first resin phantoms for near infrared spectroscopy and imaging were developed by Firbank et al [2, 3]. A number of different materials have been used to produce tissue-

simulating phantoms for optical tomography. They are (1) liquid, (2) solid (resin) plastic, (3) gelatin, (4) semi-solid silicon, and (5) solid tissue phantoms. We have designed agar-based phantoms, as shown in Figure 4.1, and resin-based solid phantoms for calibration of our fluorescent molecular tomography imaging system.

4.2 Liquid Phantoms

It is easy to create liquid-based phantoms for producing well-defined optical properties. Initially, liquid-based phantoms are made from milk or emulsified oil suspensions, which are later replaced by a lipid emulsion with the trade name of Intralipid. Liquid phantoms are made with suspensions of lipid particles that are used as scattering contrast and ink as an absorption contrast. The commercially-available lipid suspension is Intralipid. In general, for a 1% Intralipid solution, the reduced scattering coefficient is approximately $1mm^{-1}$ at 800nm; a solution with a 2mL/liter concentration of 0.2% India ink will produce an absorption coefficient of approximately 0.01 mm^{-1} at 800nm wavelength. The particle size is 10nm to 500nm. The scattering dependence can be characterized by the formula from van Staveren et al [7], which explained the power law for wavelength dependence of the reduced scattering coefficient.

There are two concerns for liquid phantoms. One is that it is necessary to hold the liquid in a container, which affects the measurement of absorption and the scattering coefficient. The container is a physical barrier, which perturbs the

light field, separating regions with different optical properties. Commercially available plastic bottles can be used to minimize this “wall” effect. The other concern is that Intralipid spoils after a few days, like milk so it cannot be used as a permanent phantom. Both of these limitations are overcome by using polyester resin solid phantoms.

4.3 Resin Solid Phantoms

Resin phantoms can be made out of polyester as described by Firbank et al. [2, 3]. These phantoms are permanent and can be shaped as desired, using standard machining equipment. For the fluorescent molecular tomography system in our lab, we have prepared resin phantoms as shown in Figures 4.1, 4.2 and 4.3. Briefly, we used titanium dioxide (TiO_2) as the scattering material. The TiO_2 particles were dispersed in ethanol. Both TiO_2 and ethanol were purchased from Sigma-Aldrich Chemical, IL. In addition, Dye-Pro jet 900NP is used as an absorption material, purchased from the Fuji Corp. The absorption coefficient of the dye was approximately 0.01/mm at 800nm. Resin with a hardener (catalyst) and mixing cups were purchased from Creative Wholesale Corporation. To prepare phantoms, we used PVC tubing as a mold for cylindrical phantoms because the PVC tube has a reduced risk of cracking. Other molds such as Tupperware® containers and Teflon® are also good for molds. Careful preparation is required for prevention of bubbles and proper curing. All work is done at the chemistry lab under a ventilation hood in the Biomolecular Imaging

Center at the VA Hospital. The recipe and mixing procedure are listed below [4, 5]. Desired amounts of TiO_2 and dye were weighed as described in the procedure. Initially, the TiO_2 and dye with ethanol were mixed well with a Sonicator. An ultrasonic bath was used for sonication of the TiO_2 and dye in Dr. Lewis's lab. Incomplete sonication of the TiO_2 and dye will result in a heterogeneous medium because sonication breaks large aggregates of titanium dioxide (TiO_2) into submicron crystallites. Once sonication is completed, it is important not to shake or stir the mixture, which might lead to aggregation. Thorough mixing of the resin and catalyst (hardener) is required to obtain a homogeneous volume that cures in a timely manner. When the catalyst (hardener) is added to the mixture of TiO_2, dye, and resin, it can be slowly mixed to minimize inclusion of air bubbles during the mixing process. There is significant heat and gas during this process. Degassing of the phantom during the initial curing process is critical because large numbers of air bubbles are embedded in the phantom mixture. Initial degassing during the curing process will produce an expansion of the resin due to the large amount of gas present. However, repeating degassing can break the bubbles and gradually reduce the phantom volume. The resin was degassed for 2 hours to remove the bubbles. It took 2 days to cure the solid resin at room temperature; if kept in oven it can be cured in a few hours.

The solid resin is a soft material that can be machined with the lathe, mill, and drill press. Care should be taken when using a saw to prevent binding of the material to the blade. Three holes were drilled into these phantoms for the

addition of 3 different concentrations of molecular probe conjugates. Saline and an Alexa Fluor 750 BBN conjugate were used as mixtures with high, medium and low concentration in the holes to allow for variable contrast studies, as shown in figure 4.2. The homogenous phantoms prepared for calibration of the FMT system are shown in Figure 4.3. These phantoms are excellent for repeatability studies as they are stable for years.

The Mie theory can be used to calculate the theoretical scattering coefficient, which was proposed by Bohren and Huffmann [6]. Figure 4.4 shows the scattering coefficient as a function of wavelength, which suggests that a long wavelength has a lower scattering coefficient.

We have prepared the phantoms for calibration and testing of our FMT system for imaging. The phantoms were found to be stable in their scattering and absorption properties.

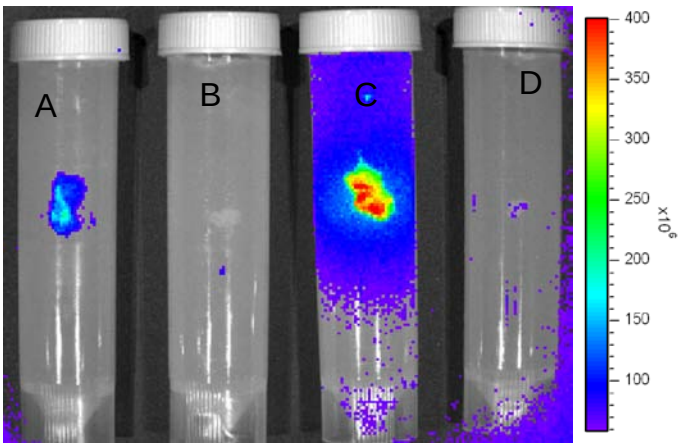

Figure 4.1: The Agar phantoms with tumors. In figure A, B they are blocking the probe in the tumor and mammary (health tissue); C, D show the uptake of the probe in the tumor and mammary.

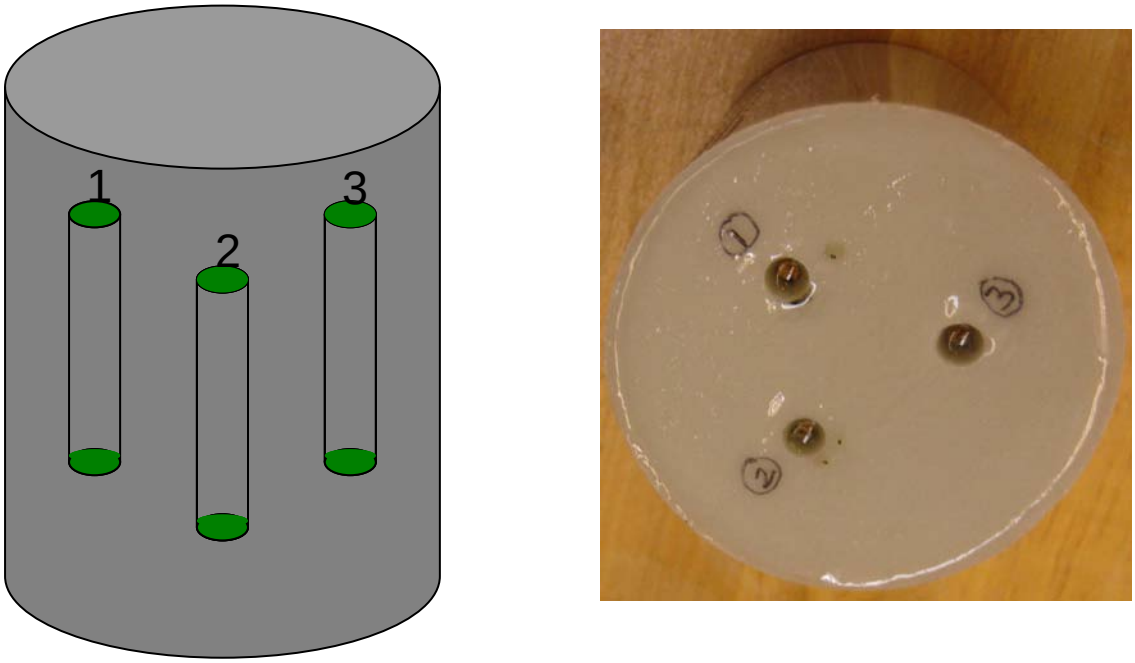

Figure 4.2: The solid resin phantom, including 3 cylinders with different concentrations of fluorophore. In the figure, above 1 is high concentration of fluorescent probe, 2 is medium concentration of fluorescent probe, and 3 is low concentration of fluorescent probe.

Figure 4.3: The homogenous phantoms.

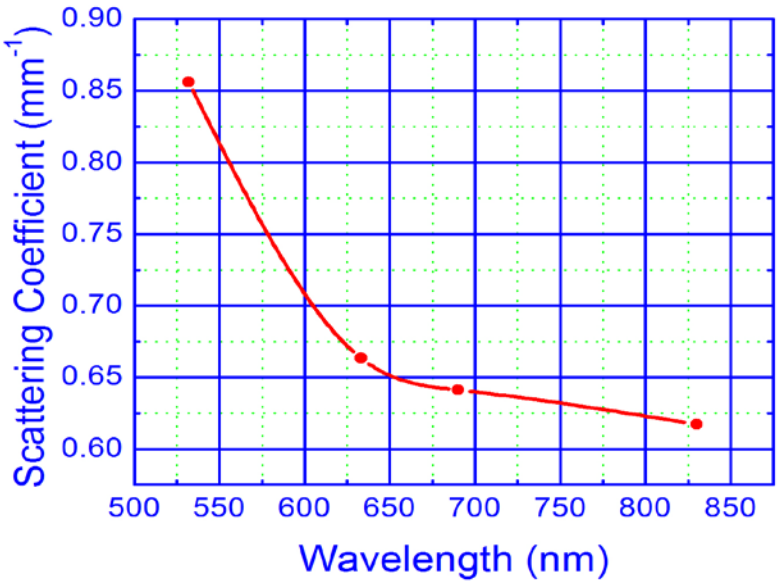

Figure 4.4: The characteristic of optical properties of the phantom. The scattering coefficient is a function of wavelength.

4.4 Recipe of Phantom Design

Materials required for preparation

1. Casting Resin
2. Catalyst(Hardener)
3. Titanium oxide [TiO_2] powder (Scatter substance)
4. Dye [Pro jet 900NP] powder (Absorption substance)
5. 100% Ethanol
6. Mold releasing substance

Equipment required

1. Test tube with cap for mixing Titanium oxide and Dye.
2. Sonicator/ Ultrasonic bath
3. Mixing cups
4. Ventilation hood
5. Molds for desired shapes like cylinders, blocks
6. Weighing machine accuracy should be 1mg

Procedure

1. Take desired amount of TiO_2 in test tube. 1 mg of TiO_2 for every 1 ml of resin will provide a transport scattering coefficient of about $0.8mm^{-1}$
2. Take desired amount of dye in test tube (same test tube of TiO_2). 0.02mg of dye for 1ml of resin will provide absorption coefficient of about 0.01 /mm
3. Add ethanol to mixture of TiO_2 and dye. The volume of ethanol should be 1% to 2% for volume of resin to be used.
4. For good mixing of ethanol, $TiO_{2,}$ and dye, use ultrasonic bath or sonicator for 20-40 minutes.
5. Take the above mixture and pour in the resin. Stir uniformly up to 1 hr.
6. Add catalyst to the above resin mixture. Stir well. For resin volumes greater than 500ml use 60 drops of catalyst. For small volumes like 100ml, use 10-20 drops.
7. Pour the above mixture in mold; let the sample cure for 12-24 hrs.
8. Remove the Solid Resin phantom; if required machine it.

Quantity of materials used for phantom preparation

- TiO_2 = 550 mg
- Dye = 11 mg
- Ethanol = 5.5 ml
- Resin = 550 ml
- Catalyst = 62 drops

Bibliography:

1. Cohen G, “Contrast detail dose analysis of six different computed tomographic scanners”. J. Comput. Assist. Tomogr, Vol. 3(2), 197-203 (1979)
2. Firbank M and Delpy DT. “A design for a stable and reproducible phantom for use in near infrared imaging and spectroscopy”. Phys. Med. Biol, Vol. 38, 847-853 (1993)
3. Firbank M, Motoki Oda and Delpy DT. “An improved design for a stable and reproducible phantom material for use in near infrared spectroscopy and imaging”. Phys. Med. Biol, Vol. 40, 955-961 (1995)
4. Recipe from Professor David Boas Harvard Medical School. Boston. USA.
5. Pogue B and Patterson M. “Review of tissue simulating phantoms for optical spectroscopy, imaging and dosimetry”. J. Bio. Opt, Vol. 11(4), 041102-41122 (2006)
6. Bohren CF and Huffman DR. Absorption and Scattering of Light by small particles. New York: Wiley (1983)
7. Hugo J Van Staveren, Moes Christian J M Moes, Jan Van Marle, Scott A Prahl, Martin Van Gemert. ”Light scattering in intralipid-10% in the wavelength range of 400-1000nm”. Applied Optics, Vol. 30(31), (1991)

Chapter 5

Summary and Future Work

In this thesis, I have described the development of a fluorescent molecular tomography (FMT) system based on fluorescent probes using a single source and detector pair that can be used for small animal imaging. I have employed the frequency domain heterodyne method in the system, which is very accurate in providing the phase and amplitude of radio frequency modulated photons in biological tissue. The results of the study demonstrate that the phase drift is 0.03° for 3 hours with a good signal-to-noise ratio. The laser source is intensity modulated, which produces a diffuse photon density wave in biological tissue, transmitted with a radio frequency signal. A radio frequency of 144 MHz is modulated with 2 kHz sinusoidal sound frequency. After passing through the biological tissue and optical system, the detection signal is sent to a receiver and the 2 kHz is demodulated. The transmitter and receiver are phase locked with a standard oscillator. The phase is detected by comparing the reference signal and the diffuse photon density wave signal from the receiver with a phase meter. The results indicate that we can obtain the phase change in a tissue phantom. We have designed solid resin phantoms and liquid phantoms for calibrating and testing our FMT imaging system.

The NIR light photons propagate deeply through tissues and excite fluorescent molecules targeted at cancerous cells. The fluorescent photons

propagate through the tissues and are detected at the surface of the sample. With NIR-excitable fluorescent contrast agents that can target cancerous cells, this method can be used to detect cancers in an early stage. We have developed an optical molecular probe with absorption peak wavelengths of 690nm, and fluorescent peaks at 783nm. The molecular probes AF 680 and AF 750 have a binding affinity to overexpressed GRPr in breast cancer cells and prostate cancer cells with cell lines T74-D and PC-3. *In vitro* results of uptake studies, internalization and receptor blocking studies show that the probes have a high binding affinity to cancerous cells. *In vivo* studies demonstrate the uptake and blocking of molecular probes in mice have high specificity and affinity to prostate and breast cancer cells. Both *in vitro* and *in vivo* studies confirm that the probes have a high binding affinity specifically and selectively to tumor tissue. The development in molecular specific targeting fluorescent contrast agents offers a high tumor to normal tissue contrast, and is capable of selectively labeling cancerous cells, thus enhancing both the sensitivity and specificity of cancer detection at an early stage.

Fluorescent molecular tomography is a promising approach for locating heterogeneity in biological tissue. The goal of this study was to develop a highly sensitive optical instrument that can non-invasively detect and locate receptor-specific probes that bind to specific receptors overexpressed in tumor cells, localized in the tumor area and several centimeters deep inside large organs such as the human breast. This system would be of benefit in the early detection

of breast tumors. It could be readily adapted through the use of other fluorescent contrast agents.

This research provides the foundation for other medical applications of the FMT system. Future research should explore the development of a system with non-contact sources and detectors. We want to develop a free-space imaging system for non-contact fluorescence molecular tomography. The system will use a diode laser to illuminate a tissue surface with incident points of light using lens-focused light beams. The diffuse photon density wave from the tissue will be collected at detectors with non-contact locations.

The FMT imaging system we developed has the potential for multimodality molecular imaging Fluorescent probes are sensitive and can be specifically conjugated for small molecules, antibodies and proteins. For over a decade, considerable progress has been made in multimodality imaging. Different imaging techniques have been combined with multimodal imaging for early stage detection of cancer. For example, PET/SPECT and CT scans have been combined to acquire functional and anatomical information. Changes in body position may result in incorrect information about the tumor. We want to combine our system with MRI imaging for simultaneous imaging of the tumor. As with MRI imaging, our system will provide high resolution images with high sensitivity.

In the future, we want to develop optical-MRI contrast agents. As described in chapter 3, it is possible to develop and evaluate AF 680 and AF 750 peptides as molecular probes. Using the same method and procedure, we will label the tumor with MRI contrast agent super paramagnetic iron oxide (SPIO)

and optical contrast agent AF750 conjugate. Simultaneous MRI and optical imaging will provide functional and anatomical information about the tumor.

GLOSSARY

Allele: The gene regarded as the carrier of either of a pair of alternative hereditary characters.

$\alpha_v\beta_3$: An integrin expressed by activated endothelial cells or tumor cells which plays an important role in angiogenesis and Metastatic tumor spread

Amino acid: An organic compound containing an amino and carboxyl group. Amino acids form the basis of protein synthesis.

Angiogenesis: Formation of new blood vessels. May be triggered by physiological conditions, like during embryogenesis or certain pathological conditions, such as cancer where the continuing growth of solid tumors requires nourishment from new blood vessels.

Annexlin V: a protein in blood which binds to phosphatidyl serin (PS) binding sites exposed on the cell surface by cells undergoing programmed cell death

Antibody: A protein with a particular type of structure that binds to antigens in a target-specific manner.

Antigen: Any substance which differs from substances normally present in the body and can induce an immune response.

Antiangiogensis: The inhibition of hew blood vessel growth and/or destruction of preformed blood vessels.

Antisense: A strategy to block the synthesis of certain proteins by interacting with their messenger RNA (mRNA). The protein synthesis is blocked by interaction of the antisense mRNA and the protein-encoding RNA.

Apoptosis: Programmed cell death. A process programmed into all cells as part of the normal life cycle of the cell. It allows the body to dispose of damaged, unwanted or superfluous cells.

Aptamer: RNA or DNA-based ligand.

Attenuation correction (AC): Methodology which corrects images for the differential absorption of photons in tissues with different densities.

Avidin: A biotin-binding protein (68 kDa) obtained from egg white. Binding is so strong as to be effectively irreversible.

Base pair: Two bases (adenine and thymine or guanine and cytosine) help together by weak bonds.

Bioinformatics: The science of managing and analyzing biological data using advanced computing techniques.

Biotechnology: A set of biological techniques developed through basic research and now applied to research and product development. In particular, biotechnology refers to the industrial use of recombinant DNA, cell fusion, and new bioprocessing techniques.

Biotin: A prosthetic group for carboxylase enzyme. Important in fatty acid biosynthesis and catabolism, biotin has found widespread use as a covalent label for macro-molecules, which may then be detected by high-affinity binding of labeled avidin or streptavidin. Biotin is an essential growth factor for many cells.

Cancer: Diseases in which abnormal cells divide and grow unchecked. Cancer can spread from its original site to other parts of the body and is often fatal.

Carrier: An individual who carries the abnormal gene for a specific condition but has no symptoms.

Cavitation: The sudden formation and collapse of low-pressure bubbles in liquids as a result of mechanical forces.

cDNA: Complementary DNA that is synthesized from an mRNA template by action of RNA-dependent DNA polymerase.

Cell: The basic structural unit of all living organisms and the smallest structural unit of living tissue capable of functioning as an independent entity. It is surrounded by a membrane and contains a nucleus which carries genetic material.

Chromosome: A rod-like structure present in the nucleus of all body cells (with the exception of the red blood cells) which stores genetic information. Normally, humans have 23 pairs, giving a total of 46 chromosomes.

Cloning: Production of cells all genetically identical from a single ancestor (production of multiple copies of a single gene or DNA segment)

Coincidence detection: A process used to detect emissions from positron-emitting radioisotopes. The technology utilizes opposing detectors that simultaneously detect two 511keV photons which are emitted at an angle of 180 degrees from one another as a result of annihilation of the positron when it combines with an electron.

DNA: Deoxygribonucleic acid: the molecule or building block that encodes genetic information.

DNA repair genes: Genes encoding proteins that correct errors in DNA sequencing.

Enzyme: A protein that acts as a catalyst to speed the rat at which biochemical reaction proceeds.

Epistasis: A gene that interferes with a prevents the expression of another gene located at a different locus.

Epitope: The specific binding site for an antibody.

^{18}F-deoxyglucose: The predominant PET imaging agent used in oncology. The deoxyglucose is trapped in cells which have increased metabolic acitivity as a result of phosphorylation. The process results in an accumulation of fluorine-18 (^{18}F) in the cells, allowing the location of cells and intensity of tumor metabolism to be determined using PET imaging.

Fluorine-18 (^{18}F): A positron-emitting radioisotope used to label deoxyglucose or other molecular probes for use as radiopharmaceuticals.

F(ab) fragment: The shape of an antibody resembles the letter Y. Antigen binding properties on both short arms. Digestion by various enzymes yields different fragments. Fragments with one binding site are called F(ab).

Fc fragment: Antibody fragment which has no binding properties (crystallizable). The Fc fragment is used by the body's immune system to clear the antibody from the circulation.

Fibrin: Fibrous protein that forms the meshwork necessary for forming of blood clots.

Fibroblast growth factor: Acidic fibroblast growth factor (alpha-FGF, HBGF-1) and basic FGF (beta-FGF, HBGF-2) are the two founder members of a family of structurally related growth factors for mesodermal or neuroectodermal cells.

Ganciclovir: An antiviral agent which is phosphorylated by thymidine kinase. As a phosphorylated substance it stops cell division by inhibiting DNA systhesis.

Gene: The fundamental physical and functional unit of heredity. A gene is an ordered sequence of nucleotides located in a particular position on a particular chromosome that encodes a specific functional product.

Gene expression: The process by which a gene's coded information is converted into the structures present and operating in the cell. Expressed genes include those that are transcribed into mRNA's and then translated into proteins, and those that are transcribed into RNAs but not translated into proteins (e.g., transfer and ribosomal RNAs).

Gene mapping: Determination of the relative positions of genes on a DNA molecule (chromosome or plasmid) and of the distance, in linkage units or physical units between them.

Gene therapy: An experimental procedure aimed at replacing, manipulating, or supplementing nonfunctional or misfunctioning genes with therapeutic genes.

Genetic code: The sequence of nucleotides, coded in triplets (codons) along the mRNA, that determines the sequence of amino acids in protein synthesis. A gene's DNA sequence can be used to predict the mRNA sequence, and the genetic code can, in turn, be used to predict the amino acid sequence.

Genome: All the genetic material in the chromosomes of a particular organism; its size is generally given as its total number of base pairs.

Genotype: The genetic constitution of an organism, as distinguished from its physical appearance (its phenotype).

Hybridization: Reversible binding of two complimentary strands of DNA or DNA/RNA to form a double stranded molecule.

ICAM: Intercellular adhesion molecules: glycoproteins that are present on a wide range of human cells, essential to the mechanism by which cells recognize each other, and thus important in inflammatory responses.

Indium-111 (^{111}In): a single photon-emitting radioisotope used to label various molecular probes for SPECT imaging.

Integrins: A specific group of transmembrane proteins that act as receptor proteins. Different integrins consist of different numbers of alpha and beta subunits. Over 20 different integrin receptors are known.

Kilobase: Unit of DNA length equaling 1,000 nucleotides.

Lectin: sugar-binding proteins which are highly specific for their sugar moieties. They bind to glycoproteins on the cell surface or to soluble gylcoproteins and play a role in biological recognition phenomena involving cells and proteins, e.g. during the immune response.

Liposome: A spherical particle in an aqueous medium, formed by a lipid bilayer enclosing an aqueous compartment.

Lysosome: A minute intracellular body involved in intracellular digestion.

Messenger RNA (mRNA): RNA that serves as a template for protein synthesis.

Microarray: Sets of miniaturized chemical reaction areas that may also be used to test DNA fragments, antibodies, or proteins.

Monosaccharide: A simple sugar that cannot be decomposed by hydrolysis.

Mutations: Change in DNA sequence.

Nucleic acid: A nucleotide polymer. There are two types, DNA and RNA.

Nucleotide: A subunit of DNA or RNA consisting of a nitrogenous molecule, a phosphate molecule, and a sugar molecule.

Oncogene: A gene, one or more forms of which is associated with cancer. Many oncogenes are directly or indirectly involved in controlling the rate of cell growth.

Peptide: A short chain of amino acids. Most peptides act as chemical messengers i.e. they bind to specific receptors.

Phage: A virus for which the natural host is a bacterial cell.

Pharmacodynamics: The study of what a drug does to the body and of its mode of action.

Pharmacokinetics: The determination of the fate of substances administered externally to a living organism e.g., the metabolism and half-life of drugs.

Transgene: A gene transferred from one organism to another.

Vector: Vehicle (virus, liposome) in which a gene can be delivered.

Virus: Noncellular biologic entity that can only reproduce in host cells.

VITA

Naresh was born in the Shalivahana family to Narasimha and Bhanumathi Kujala on 2nd October 1975 in Hyderabad, India. He was graduated with Master of Science in Physics with specialization optoelectronics with Distinction in 1998 from Osmania University, Andhra Pradesh. He then worked as assistant scientist at the Ground Instrumentation Division in the Research Center of Imrat (RCI), Govt. of India Hyderabad. Interests in teaching make him to work as fulltime Lecturer in Physics at the Brilliant Junior College, Hyderabad. In fall 2004, he went to University of Missouri, Columbia to pursue higher education. In fall 2007 he received MS in physics degree. From same University he received his Ph.D. in Physics in summer 2009. He will join as postdoctoral fellow at the Advance Photon Source in Argonne National Laboratory affiliated to Illinois Institute of Technology in August 2009.